4-2022

Fabrication and characterization of Lactobacillus Crispatus containing bioprints for bacterial vaginosis application.

Anthony J. Kyser
University of Louisville

FABRICATION AND CHARACTERIZATION OF *LACTOBACILLUS CRISPATUS*-CONTAINING BIOPRINTS FOR BACTERIAL VAGINOSIS APPLICATION

By

Anthony Kyser

B.S. University of Louisville 2020

A Thesis
Submitted to the Faculty of the
University of Louisville
J.B. Speed School of Engineering
As Partial Fulfillment of the Requirements
for the Professional Degree

MASTER OF ENGINEERING

Department of Bioengineering

April 2022

FABRICATION AND CHARACTERIZATION OF *LACTOBACILLUS CRISPATUS*-CONTAINING BIOPRINTS FOR BACTERIAL VAGINOSIS APPLICATION

Submitted By

Anthony Kyser

B.S. University of Louisville 2020

A Thesis Approved On

April 11, 2022

Dr. Jill M. Steinbach-Rankins, Ph.D.
Thesis Director

Dr. Hermann Frieboes, Ph.D.

Dr. Kunal Kate, Ph.D.

ACKNOWLEDGEMENTS

I would like to thank Dr. Steinbach-Rankins, for her guidance, steadfast commitment, and exemplary leadership that has helped me become a better researcher. I am extremely grateful for her kindness and all the time she has spent on improving me as a student. I am thankful for Dr. Steinbach-Rankins for taking me onto the bioprinting project as well. I would like to thank Dr. Mahmoud, Dr. Masigol and Kiel Butterfield for their guidance with best lab practices, as well as my lab peers for their rejuvenating inspiration and endless support. It was a great privilege to be part of a winning team.

I would like to thank the additional members on my thesis committee, Dr. Frieboes and Dr. Kate, for agreeing to lend their expertise to further strengthen my thesis from their perspectives.

I would like to thank my parents, Tom Kyser and Marian Kyser, as well as my siblings, Anna, Alex, and Rose for their loving support.

ABSTRACT

FABRICATION AND CHARACTERIZATION OF *LACTOBACILLUS CRISPATUS*-CONTAINING BIOPRINTS FOR BACTERIAL VAGINOSIS APPLICATION

Bacterial vaginosis (BV) is a condition in which healthy lactobacilli are replaced by an overabundance of pathogenic bacteria in the female reproductive tract. Current antibiotic treatments often fail to "cure" infection, resulting in recurrence in more than 50% of women, 6 months post-treatment. Recently, probiotics have demonstrated promise to restore vaginal health; however, as with other active agents, delivery requires once-to-twice daily administration. Recently, three-dimensional (3D)-bioprinting has enabled the fabrication of well-defined cell-laden architectures with tunable agent release, thereby presenting a novel approach with which to deliver probiotics. One promising bioink, gelatin alginate, was selected for study, due to its ability in other work to provide structural stability, host compatibility, viable probiotic incorporation, and nutrient diffusion. The focus of this study was to formulate and characterize 3D-bioprinted *Lactobacillus crispatus* (*L.cr.*)-containing gelatin alginate scaffolds for reproductive health applications. Different weight to volume (w/v) ratios of gelatin alginate were bioprinted to determine the formulation with the highest printing resolution, and different crosslinking reagents were evaluated for effect on scaffold integrity, via mass loss and swelling measurements. Additionally, post-print viability, sustained-release, and vaginal keratinocyte cytotoxicity assays were conducted. A 10:2 (w/v) gelatin alginate formulation was selected based on line continuity and resolution, while degradation and swelling experiments demonstrated the greatest structural stability with dual-crosslinking, showing minimal mass loss and

swelling over 28 days. Last, 3D-bioprinted *L.cr.*-containing scaffolds demonstrated sustained-release of therapeutically-relevant levels of probiotics over 28 days, while maintaining the viability of vaginal epithelial cells. For the first time, this study shows that 3D-bioprinted scaffolds may provide a new alternative to sustain probiotic delivery with future goals to help maintain or restore female reproductive health after BV infection.

TABLE OF CONTENTS

LIST OF FIGURES

INTRODUCTION

Bacterial vaginosis (BV) is the most common vaginal condition in women of reproductive age[1,2] with a global incidence spanning 23 to 29%[3]. BV is a chronic pathophysiological condition that results in an increased diversity of anaerobic and facultative bacteria, from a typically Lactobacillus-dominant state, to include increasing numbers of the taxa *Gardnerella*[4-7] and *Prevotella* within the vaginal microbiome. This imbalance of pathogenic to beneficial bacteria can result in physiological symptoms that include greyish discharge and an unpleasant odor and can further lead to serious adverse health outcomes, including increased risk of sexually transmitted infections; postsurgical infection[8,9]; cervicitis and endometritis[10,11]; pelvic inflammatory disease; cervical cancer; and preterm birth and pregnancy complications[11-24].

Treatments for bacterial vaginosis have only marginally progressed over the last fifty years[25]. Current BV treatments comprise the administration of antibiotics alone, or more recently antibiotics with adjunct probiotic treatment. While FDA-approved antibiotics, such as metronidazole, clindamycin, and tinidazole, are fairly effective in treating BV symptoms[6,26], they do not cure BV, and treatment failure rates exceed fifty percent twelve months post-infection, resulting in recurrence in 50-70% of women[2]. These outcomes are in part attributed to antibiotics decreasing both beneficial and pathogenic bacterial viability, enabling pathogenic bacteria to outcompete the growth of beneficial bacteria in the vaginal microenvironment. Furthermore, in recurrent BV cases, antibiotics are often prescribed repeatedly, promoting resistance to treatment. Together these factors

contribute to BV and abnormal vaginal flora recurrence rates as high as 66% and 84%, respectively[27].

Due to the lactobacillus-dominance typically observed in the healthy state, a potentially promising approach to modulate the vaginal microbiome is to deliver probiotics, or living microorganisms that can provide health benefits to a host. A variety of lactobacilli have been considered as promising probiotic options and are believed to exert activity by producing lactic acid and competing with anaerobes for adherence to the vaginal epithelium. The increased localized acidity provided by lactic acid decreases the surrounding pH, making the vaginal environment less hospitable to pathogen survival. In addition, probiotics may also exert combined antimicrobial and vaginal acidification effects, helping to restore balance and maintain vaginal health. Probiotics are also viewed as advantageous to other treatments due to the lack of bacterial resistance and plethora of natural bacteria to help repopulate the dysbiotic environment.

Studies have shown both oral and vaginal daily probiotic treatments to be effective in stabilizing bacterial microenvironments in a variety of pathologies, including bacterial reproductive[6,26,28] and bacterial vaginosis infections[29-33]. Available dosage forms include topical creams, daily oral supplements, or daily to twice daily vaginal capsules, tablets, or suppositories[5,25,28,34-37]. While oral treatments have been shown to deliver probiotics to the vagina, localized intravaginal delivery is often favored to increase bioavailability and direct colonization[25,28,38-43]. A variety of probiotic dosage forms have demonstrated clinical efficacy in BV treatment[32,35,44-46]. As one example, vaginal capsules and tablets, loaded with $10^8 – 10^9$ colony forming units (CFU) of either one or multiple *Lactobacillus* strains, taken one to two times a day, resulted in doubling the clearance rate of BV infection[5,25,47].

In addition, probiotics have been administered subsequent to antibiotic regimens to help restore the vaginal environment with beneficial bacteria after BV infection. One study administered oral clindamycin for seven days, followed by vaginal probiotic capsules for seven days (10^9 *Lactobacillus casei rhamnosus* (LCR35)). After one month, 83% of patients were reported as "cured" relative to 35% in the control group[5]. Recently, one of the most promising options has been shown in staging the delivery of probiotics with the antibiotic metronizadole, showing a decrease in BV recurrence and increased efficaciousness in eliminating BV, relative to antibiotic-only treatment[5,6,26,28,48].

Despite alleviating initial symptoms and helping to restore the healthy vaginal environment, challenges exist with current probiotic (and antibiotic) dosage forms, which rely on frequent daily administration to obtain therapeutic effect. These dosing regimens may be inconvenient for many women, and lead to a lack of compliance that has adverse effects on efficacy. Additionally, barriers to convenience and ease-of-use, such as messiness, leakage, and unfavorable discharge, impact user adherence and treatment efficacy[5,7,42,49-52]. Relative to the transient administration provided by tablets, suppositories, creams, and gels, one of the few platforms that has been designed to sustain probiotic[31,53-57] (and other active agent[53,58,59]) delivery is the intravaginal ring (IVR). To our knowledge, pod-based IVRs containing lyophilized *L. gasseri*, are the only technology designed to-date to provide localized and sustained probiotic delivery *in vitro*[60].

Relative to the mold-based and often multi-step techniques typically involved in IVR fabrication, 3D-bioprinting enables the rapid manufacturing of scaffolds that have historically been used to support or viably incorporate mammalian cells for a variety of biomedical applications. While bioprinted scaffolds have been more frequently developed

as cell scaffolds, a variety of bioinks have incorporated different cell types in a high-throughput method[61,62]. In particular, bioinks composed of gelatin and alginate have been shown to promote high cell viability, scaffold stability, nutrient diffusion, and co-delivery of multiple agents[63-66]. In parallel, technical advances have enabled the printing of diverse materials in spatially distinct layers to provide temporally modulated delivery regimens. Moreover, successes in attaining cell proliferation and differentiation for tissue engineering applications indicate significant potential for probiotic cells to similarly undergo proliferation with the potential for probiotic "release" from the scaffold and concomitant restoration of a healthy vaginal environment. Yet, to date, few studies have incorporated prokaryotic cells during scaffold bioprinting[67-74].

Given the lack of probiotic-containing sustained-delivery dosage forms, the goal of this study was to develop a new 3D-bioprinted dosage form to enable viable and prolonged probiotic delivery. In this study, we evaluated scaffold formulation, printability, degradation, and probiotic proliferation and release kinetics from the scaffold. Ideal design criteria of 3D-bioprinted constructs included high line resolution with minimal line agglomeration, structural stability, high bacterial viability, and sustained probiotic release and/or proliferation at therapeutically relevant concentrations for a minimum of one week. We anticipate that these studies will provide a foundation for future sustained-release probiotic delivery vehicle design, to eventually provide an alternative approach to treating BV and restoring vaginal health.

MATERIALS AND METHODS

2.1 Materials

Lactobacillus crispatus (MV-1A-US) was purchased from BEI Resources. De Man, Rogosa, and Sharpe (MRS, Sigma 69966) broth; simulated vaginal fluid (SVF) composed of NaCl, KOH (Sigma, P-6310), $Ca(OH)_2$ (Sigma, 31219-100G), bovine serum albumin (Fisher, BP1600-100), lactic acid (Alfa Aesar, 36415), acetic acid (Fisher, A38-500), glycerol (VWR, M152-1L), urea (Alfa Aesar, A12360), and glucose (Sigma, G7021-1Kg); and phosphate buffer solution (PBS) composed of NaCl (VWR, 0241-1kg), KCl (Fisher, P217-500), Na_2HPO_4 (Sigma, S9763-100G), and KH_2PO_4 (Sigma, P5655-100G) were purchased to formulate release eluants. Genipin and calcium chloride ($CaCl_2$) were obtained from Sigma Aldrich (St. Louis, MO). Simulated vaginal fluid was prepared as mentioned in[75].

2.2. Probiotic Culture

L. crispatus was initially cultured on MRS (supplemented with 0.1% Tween 80) agar plates under anaerobic conditions at 37°C, and colony formation was observed after 48 hr. *L. crispatus* was then sub-cultured by selecting a single colony from the agar plates and culturing in 1 mL of MRS broth in a closed microcentrifuge tube at 37°C for an additional 48 hr. Subsequent sub-cultures were established by diluting 200 µl of *L. crispatus* with 9.8 mL of MRS broth (1:50).

2.3 Bioink Preparation and Probiotic Incorporation

Bioinks were formulated from gelatin from bovine skin (Sigma, G9391-100G) and sodium alginate (MP Biomedicals, 218295). Several different ratios of gelatin to alginate were tested, as most literature sources utilized 10 to 20% w/v gelatin and 1 to 5% w/v alginate to print mechanically stable constructs[66,76-78]. MRS broth was used to dissolve the gelatin and sodium alginate in ratios of 10:1, 10:2, 11:2, 12:2, and 16:4 (w:w)/volume of MRS (hereafter w/v), followed by overnight incubation at 37°C. Bioinks were then removed from the incubator, vortexed, and rested for 5 min before transferring to a syringe for subsequent bioprinting.

To fabricate *L. crispatus*-containing scaffolds, a *L. crispatus* sub-culture was diluted 1:10 in PBS. A Nanodrop 2000 (Thermo Scientific, MA) was utilized to measure the absorbance value (OD_{600}) to determine the volume of *L. crispatus* solution to add to the bioink, using the equation $y = ((9 \times 10^7) * (x)) - 2 \times 10^7$ to obtain a theoretical loading of 5×10^7 CFU per mg scaffold. The appropriate volume of *L. crispatus* solution was centrifuged (3500 × g, 10 min), supernatant was removed, and the pellet was resuspended in 500 µL of MRS. The bacteria were then added to 4.5 mL of prepared bioink and the bacteria-bioink mixture was transferred to a syringe for bioprinting. The CORE head of an Allevi 3 Bioprinter (Allevi, Inc., Philadelphia, PA) was heated to 37°C prior to bioprinting.

2.4 Bioprinting and Crosslinking of the Scaffolds

The Allevi 3 Bioprinter was used to bioprint blank and *L. crispatus*-containing scaffolds. The 3D bioprinter was calibrated, and processing parameters including extruder temperature, pressure, and printing speed were optimized for printing.

The extruder temperature was set at 37°C to decrease bioink viscosity and to simulate the physiological environment, while the initial extruding pressure was adjusted between 32 and 42 psi[79]. Gelatin to sodium alginate ratios of 10:1, 10:2, 11:2, 12:2, and 16:4 w/v were initially printed in layer thicknesses of 200 µm with a 30G (152 µm inner diameter) needle to determine the printing formulation that provided the most accurate line resolution. Bioinks were loaded into 1 mL plastic syringes with a spatula, the syringe was placed in the extruder, and five different line formulations were printed to assess printing feasibility and resolution.

An extruded bioink formulation that displays consistent dimensions with the print files will validate and enable the printing of more complex architectures. After determining the formulation that resulted in bioprints with accurate measurements of the desired construct, the needle gauge was varied to determine the effect on line resolution. Bioinks formulated in a 10:2 w/v ratio were printed with a 26, 30, or 34-gauge luer lock needle attached to the syringe. The pressures and extrusion rates were adjusted to adapt to the changes in shear stress resulting from different needle diameters. Circle-shaped lattices were printed with diameters of 30, 15, and 8 mm to determine resulting print resolutions with different needle gauges. Additionally, for each different lattice diameter/needle combination, scaffolds were printed with 1, 2, and 3 mm thicknesses. These circular lattice structures were printed with pre-made GCODE files that specified print dimension and geometry.

Printing parameters, determined from these experiments, were used to inform and fabricate subsequent intravaginal ring-type designs. The high-resolution circle-shaped lattice prints helped to inform the needle gauge needed to print a simpler, more application appropriate intravaginal ring shape.

After determining the optimal parameters of formulation and needle gauge that best represented the input dimensions of diameter, line width and thickness, scaffolds were printed in intravaginal ring-shaped geometries to represent currently accepted dosage forms. The IVR scaffolds were printed using a customized STereoLithography (STL) file specifying an outer diameter of 4 mm and inner diameter of 3 mm. The optimized bioink used for printing contained 5 x 10^7 CFU/mg of *L. crispatus* at a 10:2 gelatin to sodium alginate ratio. The homogenous bioink was transferred to the bioprinting syringe at a volume of 1 mL. Prior to printing, the CORE head of the Allevi 3 bioprinter was heated to 37°C to maintain an ideal physiological environment for *L. crispatus*. The extruder pressure was adjusted to 42 psi for a 30G needle to print constructs with accurate dimensions stated in the printing file.

Subsequent to printing, both blank and *L. crispatus* containing IVR-shaped scaffolds were placed in the refrigerator (4°C) for 15 min to harden. Two different crosslinkers, genipin and $CaCl_2$, were then used to crosslink the gelatin and alginate portions of the scaffold, respectively. Genipin has been shown to improve the mechanical and thermal properties of gelatin while maintaining drug permeation capabilities[80], as well as prolonging its degradation time[81], while $CaCl_2$ relies on ionic crosslinking to form a

stable three-dimensional network providing mild reaction conditions, greater aqueous permeability, and increased stability of alginate after immersion in solute[82-84].

A variety of crosslinking conditions were evaluated to assess the effect of crosslinking molecule and time on scaffold integrity and probiotic viability: genipin-only (4 hr), genipin-only (24 hr), $CaCl_2$-only (20 min), $CaCl_2$ (20 min) and genipin (4 hr), and $CaCl_2$ (20 min) and genipin (24 hr). Uncrosslinked scaffolds were made for comparison to the crosslinked groups. For dual-crosslinked scaffolds, $CaCl_2$ crosslinking was conducted prior to genipin crosslinking. Briefly, 20 mL of 10% w/v $CaCl_2$ in DI water were poured on the chilled scaffolds in a petri dish and scaffolds were chilled at 4°C for 20 min. Next, 5 mL of 0.5% w/v[80,85] genipin in 1x PBS was poured on the chilled scaffolds and incubated at room temperature for 4 or 24 hr[86]. Crosslinked scaffolds were then washed three times with DI water and placed back in the refrigerator until use. For $CaCl_2$-only or genipin-only crosslinked control groups, scaffolds were crosslinked and incubated for the durations and temperatures defined above.

2.4 Viscosity

Bioink viscosity was determined for the 10:2 w/v blank and *L. crispatus*-containing gelatin alginate formulations to ensure consistent bioink extrusion and resulting mechanically stable scaffolds. Similarly, 16:4 w/v bioinks served as a control group to compare difficult-to-print formulations. A DVE viscometer (AMETEK Brookfield, MA) was used to assess bioink viscosity and a rechargeable temperature data logger (Omega, CT) was used to measure the temperature with respect to time. Initially, 10 mL of the 10:2

gelatin alginate bioink was aliquoted to a scintillation vial and incubated at 37°C. The S63 spindle was submerged into the bioink with spindle top 1 mm above surface, and temperature sensors were placed in the bioink to simultaneously record changes in viscosity and temperature. The viscometer was set to 20 rpm, and the viscosity was measured as a function of temperature.

2.5 Degradation and Swelling

To assess mass loss, crosslinked scaffolds were dried at 50°C overnight to ensure scaffolds were fully dry, and the initial dry weight of the samples (W_i) was measured. Scaffolds were then immersed in 1.5 mL of SVF for 0, 4, 8, 24, 72, 120, and 168 hr, and 2, 3, and 4 wk, after which the final sample weight (W_f) was measured. The mass loss percentage were determined according to Eq. (1):

$$\text{Mass Loss Percentage} = [(W_i - W_f)/W_i] \times 100 \quad (1)$$

To assess scaffold swelling, the initial mass of the crosslinked scaffolds (W_i) was measured. Scaffolds were then placed in microcentrifuge tubes containing 1.5 mL SVF. Scaffold weights were evaluated at 0, 24, 48, 72, 96, 120, 144 and 168 hr, and 2, 3, and 4 wk. At each time, scaffolds were removed, dried, and weighed to obtain the corresponding weight (W_s). The percent of mass change relative to initial mass was determined according to Eq. (2):

$$\text{Mass Swelling Percentage} = [(W_s - W_i)/W_i] \times 100 \quad (2)$$

2.6 Initial Loading and Viability of Bacteria

After bioprinting, uncrosslinked blank and *L. crispatus*-containing scaffolds were assessed for loading after crosslinking for 0, 25, and 60 min at 4°C, conditions relevant to $CaCl_2$ crosslinking. Then pre-weighed samples were placed in 1 mL MRS broth at 37°C. After scaffold dissolution, the tubes were gently vortexed and the 20 µL was serially diluted in 180 µL MRS broth. Aliquots of 5 µL were plated on MRS agar plates, placed in the anaerobic chamber for 48 hr, and the number of CFUs was counted.

2.7 Quantification of Probiotic Release and Proliferation from Printed Scaffolds

The release and proliferation of *L. crispatus* from crosslinked scaffolds were evaluated in MRS broth for up to 4 wk. Pre-weighed scaffolds were placed in 1.5 mL microcentrifuge tubes and incubated in 1.5 mL MRS at 37°C with constant shaking at 150 rpm. The supernatant of each sample was removed after 0, 4, 8, 24, 72, 120, 144, and 168 hr, and 2, 3, and 4 wk, and sample eluate was diluted by adding 20 µL of sample to 180 µL of MRS broth. Five µL of each sample dilution were plated on MRS agar plates and placed in an anaerobic chamber for 48 hr. After 48 hr, the plates were evaluated for CFU counts. After each collection, the scaffolds were washed four times in 5 mL PBS, placed in 1.5 mL fresh MRS broth, and incubated until the next time point.

2.8 Quantification of Lactic Acid and pH

Scaffold release eluates, collected at the corresponding probiotic release time points (0, 24, 48, 72, 96, 120, 144, and 168 hr, and 2, 3, and 4 wk) were evaluated for lactic acid

production and resulting pH change. Briefly, 1 mL of eluate was centrifuged at 2500 x g for 5 min to separate the bacteria from the solution and then the solution was serial diluted using 10-fold dilutions. The concentration of L- and D-lactic acid was determined with a lactic acid detection kit (R-biopharma; Darmstadt, Germany) and the corresponding pH of eluates at each time point was measured using pH strips with a pH range of 1 to 6 and an accuracy of 0.5 pH units (Fisher Scientific).

2.9 Probiotic Stability in Bioprinted Scaffolds after Storage

The temperature stability of *L. crispatus* formulated in 10:2 gelatin:alginate bioprinted scaffold was tested by CFU counting on MRS agar, as described above. Scaffolds containing *L. crispatus* were stored in sealed Petri dishes at either -20°C, 4°C, or 20°C, and probiotic viability evaluated for up to 4 wk. After 1, 2, and 4 wk, the stored bioprinted scaffolds were placed in microcentrifuge tubes and incubated in fresh 1.5 mL MRS broth for 30 min at 37°C with constant shaking at 150 rpm to assess daily release from the scaffold. The release was then diluted using 10-fold serial dilutions, 5 µL was plated on MRS agar plates, and CFUs were counted after 48 hr of anaerobic incubation at 37°C.The cumulative release and proliferation of *L. crispatus* in MRS from scaffolds were evaluated for and compared to scaffolds assessed immediately post-fabrication.

2.9 Scaffold Morphology

The morphology of the blank and *L. crispatus*-containing scaffolds was characterized using scanning electron microscopy (SEM). Scaffold cross-sections were placed on carbon tape, sputter-coated with a layer of palladium/gold alloy (8.5 nm), and

imaged using Apreo C LoVac Field Emission SEM (Thermo Scientific, Waltham, MA). Proliferation was compared in scaffolds that were immersed in timepoints at 0, 1, and 7 days in MRS and SVF.

2.10. VK2/E6E7 Viability

An MTT assay was used to determine the preliminary in vitro safety of $CaCl_2$ and genipin crosslinked, blank and *L. crispatus*-containing scaffolds, in a VK2/E6E7 cell line. Cells were plated at a density of 300,000/well in a 12-well plate and incubated for 24 hr at 37°C. Media only (untreated cells) and 10% DMSO were used as viable and non-viable cell controls. After 24 and 72 hr incubation, 100 µL of MTT labeling reagent was added to each well and incubated at 37°C for 4 hr, followed by adding 100 µL of lysis buffer containing 10% sodium dodecyl sulfate and 0.01 M hydrochloric acid. After 16 hr incubation, the absorbance was read at 570 nm (SYNERGY Microplate Reader, Biotek Instruments Inc) and normalized to cell-only absorbance to attain the relative percent of cell viability.

2.10 Statistical Analysis

All experiments were done in triplicate, and Minitab (Minitab, LLC, State College, PA) and GraphPad (GraphPad Software, La Jolla, CA) were used in statistical analysis. Three replicates were used for each sample and were subjected Grubbs' test ($p \leq 0.05$) to determine outliers. All statistical analyses in GraphPad Prism (version 9.3.1) were performed using one-way ANOVA with the Tukey multiple comparison's test ($p \leq 0.05$).

RESULTS

3.1 Bioprinting Probiotic Scaffolds

The optimal bioink formulation and printing parameters were determined by evaluating the printing resolution, mechanical integrity, and probiotic loading in probiotic-containing scaffolds. The bioink formulation ratio was varied to assess its impact on line resolution and scaffold integrity with a standard-gauge needle after printing.

First, the line resolutions of blank and *L. crispatus*-containing gelatin:alginate (10:1, 10:2, 11:2, 12:2, 16:4 (w:w)/v (hereafter w/v) formulations were evaluated (**Figure 1**). An image of the Allevi bioprinter and bioprinted lines resulting from initial prints are shown in **Figure 1A** and **B**. Overall, the 10:2 and 12:2 w/v blank formulations were found to provide the most line continuity and closest line resolution relative to input dimensions, whereas the 10:1 and 11:2 formulations resulted in thicker and thinner lines, respectively. In comparison, the 16:4 formulation resulted in some line fragmentation, with an overall asymmetrical and jagged line appearance.

Upon addition of *L. crispatus*, the 10:1, 11:2, and 12:2 w/v formulations resulted in line broadening, in addition to line fragmentation and inconsistent extrusions, while the 16:4 w/v formulation continued to display asymmetrical and jagged morphology. Overall, the 10:1, 11:2, and 12:2 w/v prints showed a 2-fold increase in width when *L. crispatus* was incorporated (spanning ~0.90-1.65 mm, with respect to the input line width of 0.68 mm), contributing to a decrease in line resolution. In contrast, the 10:2 w/v blank and *L.*

crispatus-containing bioinks exhibited the finest line resolution and ability to maintain structural integrity after *L. crispatus* incorporation, with line widths of 0.76 ± 0.06 mm and 0.78 ± 0.03 mm, respectively, corresponding to a design specification of 0.68 mm. Therefore, the 10:2 formulation was selected for subsequent studies.

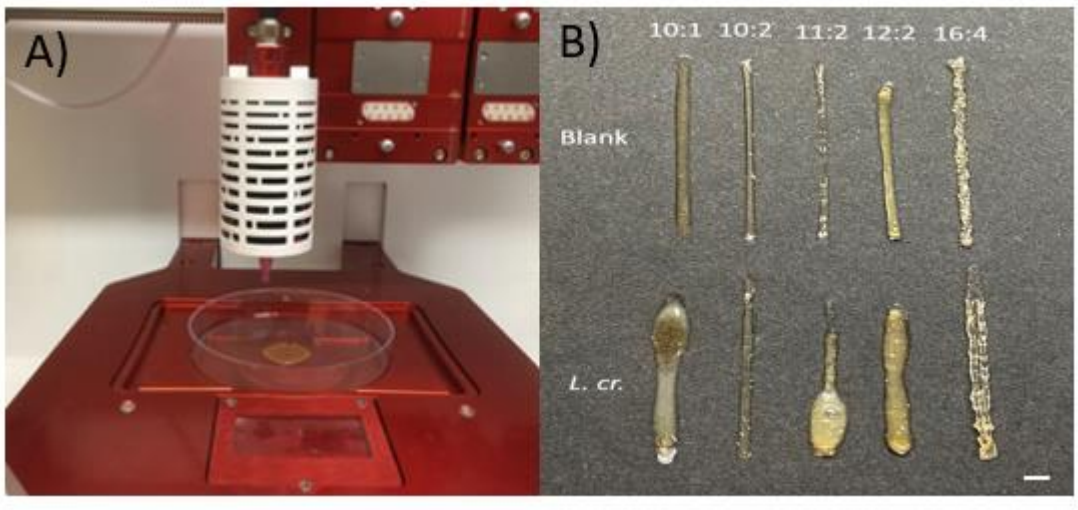

FIGURE 1: EXPERIMENTAL SETUP AND LINE RESOLUTION

Figure 1. Experimental setup and representative images of gelatin alginate scaffolds bioprinted with different formulation ratios. (A) Image of the Allevi 3D bioprinting setup and components. Briefly, the bioink is loaded into a dispensing syringe that is attached to a luer-locked needle in the CORE head and extruded into a petri dish. (B) Representative line prints of the 10:1, 10:2, 11:2, 12:2, and 16:4 w/v blank and *L.cr.*-containing gelatin alginate formulations extruded at 42 psi and 37°C with a 30G needle, shown immediately post-print. Coded file line width was defined as 0.68 mm. The 10:2 ratio provided line resolutions closest to CAD drawing specifications for both the blank and *L. cr.*-containing scaffolds. Scale bar represents 1 mm.

Next, the effects of needle gauge and *L. crispatus* addition were evaluated for the 10:2 formulation. A variety of circle-shaped lattice structures were printed with varying diameters and thicknesses, with 26G, 30G, and 34G needles (**Figure 2**). Blank and *L. crispatus*-containing bioprints are shown in **Figures 2A-D** and **2E-H**, respectively. Scaffold diameter and thickness were varied between 8, 15, and 30 mm and 1, 2, and 3 mm (here, for each 3x3 panel).

Overall, uniform bioink extrusion was achieved using pressures of 42 and 115 psi and 30G and 34G needles, respectively, while well-defined structures were unachievable, in particular for *L. crispatus*-containing with the larger 26G needle, regardless of the pressure. For most bioprints, the 34G needle maintained infill spaces and resolution of both blank and *L. crispatus*-containing lattice structures, whereas the 26G and 30G needles resulted in amorphous lattice structures for the *L-crispatus*-containing lattice structures. Based on these observations, the 34G needle was used to print subsequent scaffolds.

In parallel, printing integrity was evaluated as a function of *L. crispatus* loading (10^7, 10^8, and 10^9 CFU per mg scaffold) as a function of scaffold thickness and diameter (**Figures 2I and J**). The thicknesses and diameters of the resulting scaffolds were measured at 4 different positions within the circle-shaped structures as a function of probiotic concentration. Generally, as probiotic concentration increased, scaffold thickness and diameter increased (**Figures 2I and J**). As one example, 8 mm diameter scaffolds printed with thicknesses of 2 mm, showed an initial thickness of 1.82 mm for blank scaffolds, subsequently increasing to 1.92, 2.05, and 2.31 mm for 10^7, 10^8, and 10^9 CFU *L. crispatus*

per mg scaffold. Additionally, as the input scaffold thickness increased from 1 to 3 mm, the deviation in thicknesses increased for blank and *L. crispatus*-containing formulations, signifying less accuracy in print resolution.

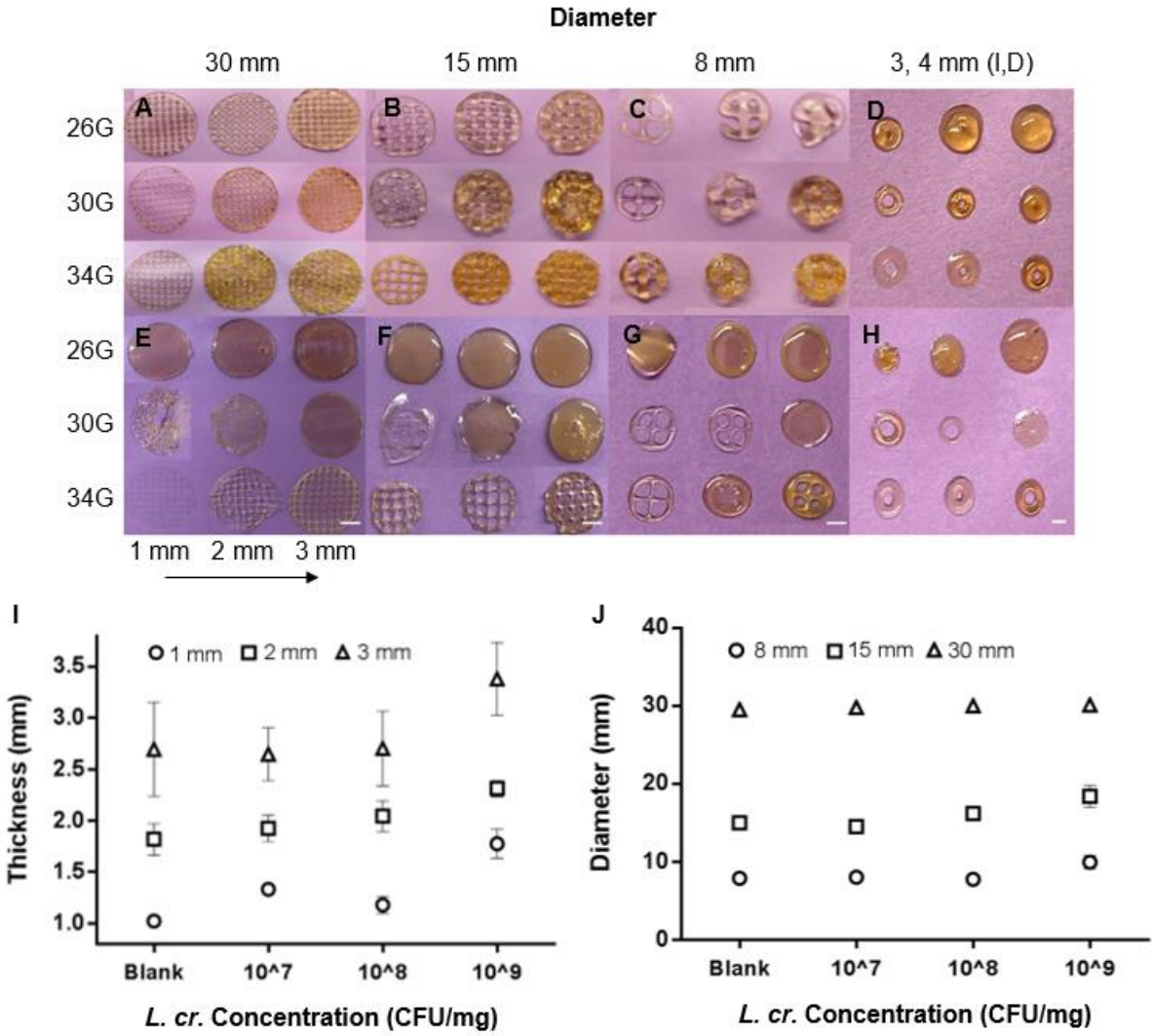

FIGURE 2: REPRESENTATIVE IMAGES OF SCAFFOLDS

Figure 2. Representative images from (A-D) blank and (E-H) *L. crispatus*-containing scaffolds that were bioprinted using a 10:2 w/v gelatin alginate bioink. Scaffolds were printed using 26, 30, and 34G needles and extrusion pressure was adjusted to compensate

for different needle gauges. Blank or *L. crispatus*-containing scaffolds were printed with (A, E) 30 mm, (B, F) 15 mm, and (C, G) 8 mm diameters. Within each panel, the input thickness of printed scaffolds increased from 1 to 3 mm (left to right). Panels D and H show blank and *L. crispatus*-containing ring structures fabricated with 3 and 4 mm ID/OD. Scale bars represent 10, 5, 3 and 2 mm from left to right. The reproducibility in (I) thickness and (J) diameter of blank and *L. crispatus*-containing scaffolds were measured as a function of probiotic incorporation. Panel I shows the measured thicknesses from 8 mm diameter scaffolds printed with 1, 2, and 3 mm thicknesses. Panel J shows the measured diameters from 1 mm thick scaffolds printed with 8, 15, and 30 mm diameters.

Somewhat similar trends were observed for 1 mm thick scaffolds printed with a 15 mm diameter. The average printed diameter of 15 mm scaffolds increased from 14.97 mm, for blank scaffolds to 14.52, 16.18, and 18.38 mm for scaffolds containing 10^7, 10^8, and 10^9 CFU *L. crispatus* per mg scaffold. Scaffolds printed in 8 and 30 mm diameters showed minimal changes in diameter as a function of probiotic incorporation, with statistical significance observed only for the 8 mm diameter scaffolds (blank to 10^9 CFU/mg). Overall, scaffolds containing 10^7 CFU/mg provided the closest lattice print dimensions in both thickness and diameter to blank scaffolds. Moreover, the impact of *L. crispatus* concentration was more significant when considering thickness of scaffolds, leading to less reproducibility and maintenance of line resolution at increased scaffold thicknesses and probiotic concentration. To maximize loading, while still achieving printing accuracy, subsequent scaffolds were printed with $5x10^7$ CFU *L. crispatus*/mg.

3.2 Viscosity

Bioink viscosity was evaluated as a function of temperature for the 10:2 and 16:4 w/v (control) blank and *L. crispatus*-containing formulations, due to the temperature dependence of probiotic viability. At 37°C, the viscosities of 10:2 w/v blank and *L. crispatus*-containing (5 x 10^7 CFU/mg) gelatin alginate bioinks were 1171 ± 17 cP and 1616 ± 19 cP, respectively. As the temperature decreased from 37°C to 28°C, both blank and *L. crispatus*-containing 10:2 formulations showed steady increases in viscosity, resulting in viscosities of 1989 ± 23 and 2501 ± 19 cP, respectively. (**Supplementary Figure 1**). Similar trends were observed with the 16:4 w/v formulation, however the initial viscosities (at 37°C) of blank and *L. crispatus*-containing (5 x 10^7 CFU/mg) bioinks were much higher with values of 154,500 ± 13,352 and 125,167 ± 1,258 cP. As the temperature decreased from 37°C to 30°C, blank and *L. crispatus*-containing 16:4 formulations showed an initially steady increase in viscosity, after which the *L. crispatus*-containing bioink showed a sharp increase in viscosity. At 28°C, the blank and *L. crispatus*-containing bioinks had viscosities of 270,000 ± 27,839 and 507,167 ± 55,219, respectively. Overall, both the 10:2 and more viscous, 16:4, formulations showed similar trends of increasing viscosity as a function of decreasing temperature; however, the 16:4 formulation exhibited more than a 100-fold increase in initial and final viscosities.

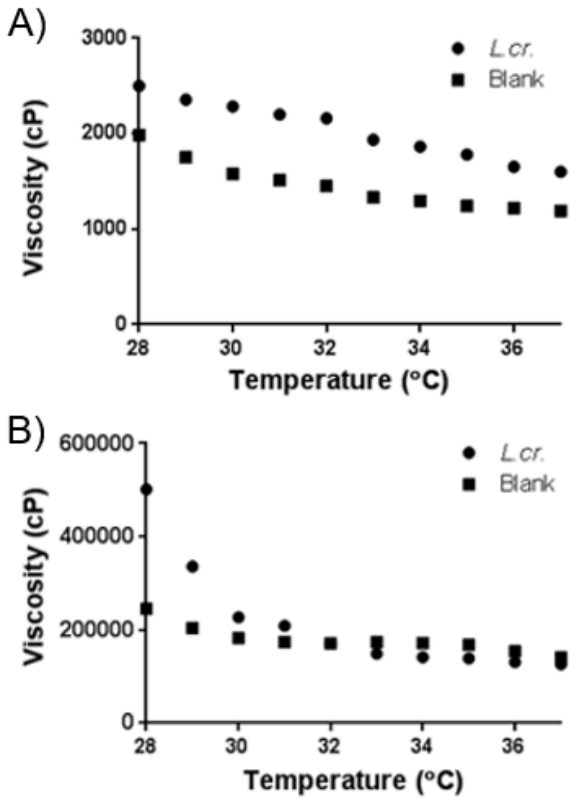

SUPPLEMENTARY FIGURE 1: VISCOSITY OF BIOINKS

Supplementary Figure 1. The viscosity of (A) 10:2 and (B) 16:4 w/v gelatin alginate formulations shown from 28°C to 37°C. Viscosity was measured every 1°C.

3.3 Scaffold Degradation and Swelling as a Function of Crosslinking Conditions

Multiple crosslinking conditions were evaluated to determine the crosslinking conditions and duration that resulted in the least mass loss and degradation (**Figure 3**). Dual-crosslinking with $CaCl_2$ followed by genipin was found to be the most resistant to degradation over 28 days (**Figure 3A**), while crosslinking solely with $CaCl_2$ (data not shown) or genipin-only resulted in degradation within 1 or 7 d, respectively. Furthermore,

scaffolds crosslinked with genipin-only were fully degraded within 7 d, independent of 4 or 24 hr crosslinking duration. Similarly, dual-crosslinking with both $CaCl_2$ and genipin for only 4 hr resulted in rapidly degraded structures, on the order of 7 d, while dual-crosslinking for 24 hr resulted in intact structures over 28 d (**Figure 3A**).

In parallel with macrostructural observations, scaffold degradation was quantified by measuring the mass loss of oven-dried scaffolds with respect to time (**Figure 3B**). The average mass of the dual-crosslinked scaffold printed with 5×10^7 CFU *L. crispatus*/mg was 2.21 ± 0.25 mg. Overall, initial mass loss occurred within the first 4 to 8 d, and stabilized after these durations. After 24 hr, dual-crosslinked and genipin-only crosslinked scaffolds (crosslinked for 24 hr) lost 16 and 19% of their initial masses, respectively. After 28 d, small differences in mass loss were observed between dual- and genipin-only crosslinked scaffolds ($p \leq 0.0001$), with total mass losses of 25% and 38% of initial masses, respectively.

In parallel with mass loss measurements, scaffold swelling was quantified by measuring the mass of tissue-blotted scaffolds relative to their initial mass (**Figure 3C**). After 24 hr, dual-crosslinked scaffolds exhibited 18% mass loss, relative to the 24% mass loss observed after crosslinking with genipin-only. After 28 d, both dual- and genipin-only crosslinked scaffolds showed mass losses of 45%. Overall, minimal differences in scaffold swelling, as measured by mass change, were observed between dual- and single-crosslinked groups.

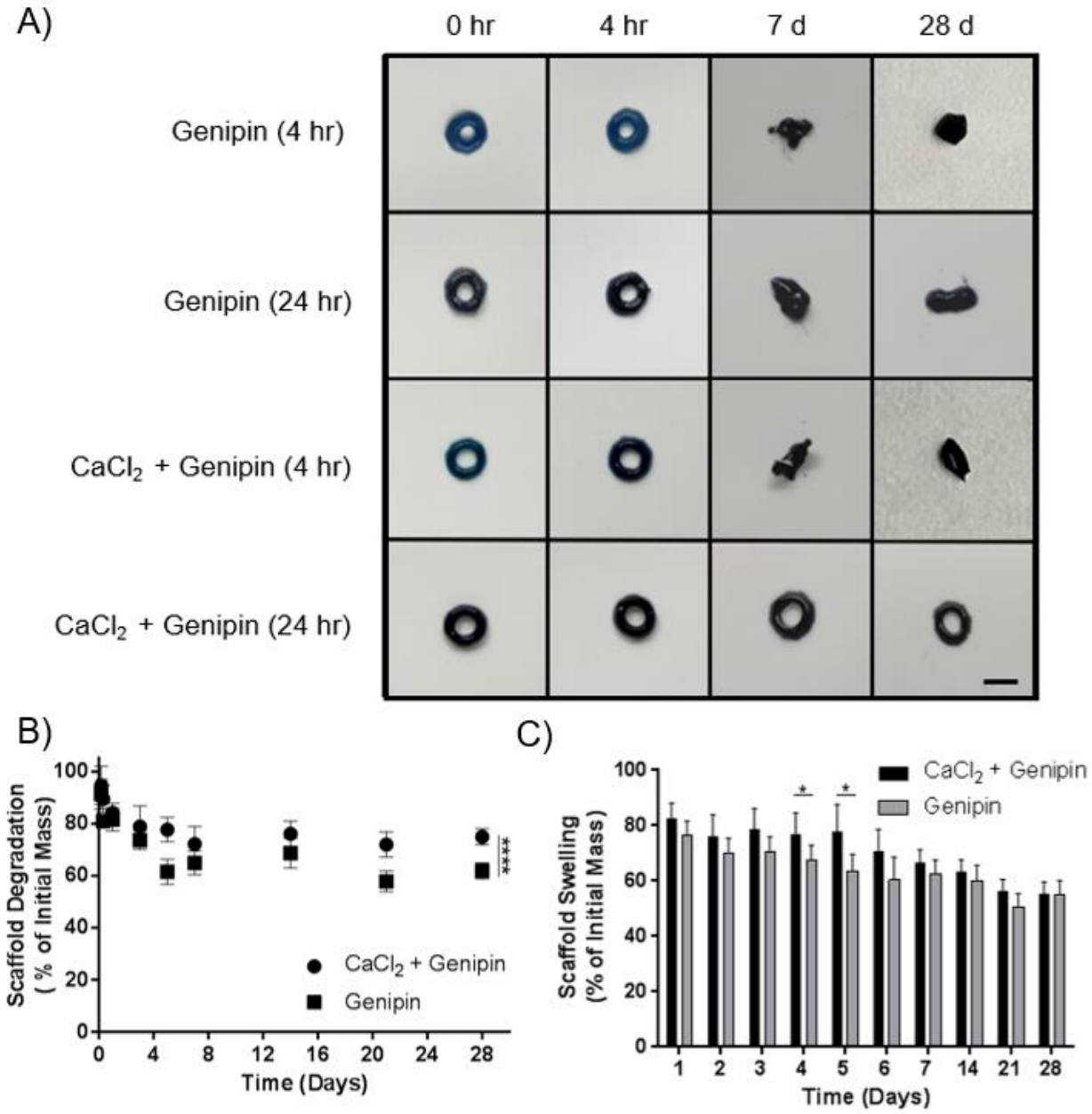

FIGURE 3: SCAFFOLD DEGRADATION AND SWELLING

Figure 3. Scaffold degradation and swelling were evaluated as a function of crosslinker and crosslinking duration. (A) Representative images of ring-shaped *L. crispatus*-containing scaffolds (OD: 4 mm, ID: 3 mm) printed with 5×10^7 CFU *L. crispatus* per mg

scaffold and crosslinked with genipin-only or both $CaCl_2$ and genipin for 4 or 24 hr. Scaffold macrostructure was evaluated after incubation in 5 mL MRS media after 0 and 4 hr, and 7 and 28 days. Scale bar represents 4 mm. Scaffolds printed with $CaCl_2$-only dissolved immediately upon exposure to media (not shown). (B) Scaffold mass loss, attributed to degradation, and (C) scaffold swelling, both shown as the percent of initial mass, for scaffolds dual-crosslinked with $CaCl_2$ and genipin or genipin-only for 24 hr, were evaluated for 28 d in SVF. Degradation and swelling (mass loss) values are shown as the mean ± standard deviation from five independent ring scaffolds. Statistical significance between experimental groups, as calculated by one-way ANOVA, is represented by *$p \leq 0.05$ and ****$p \leq 0.0001$.

3.4 *L. crispatus* Viability and Release

Bioprinted scaffolds containing $1x10^7$, $5x10^7$, and $1x10^8$ CFU *L. crispatus* per mg scaffold were evaluated for probiotic viability after 0, 25, 60 min. at 4°C to evaluate the impact of potential $CaCl_2$ crosslinking durations on probiotic viability (**Figure 4A**). The *L. crispatus*-containing scaffolds maintained *L. crispatus* viability at each loading concentration, independent of crosslinking duration at 4°C. Overall, a slight increase in viability was observed between the unprinted blank scaffold control group and blank scaffolds crosslinked for 0, 25, or 60 min durations ($p \leq 0.01$). Furthermore, it is visually evident that the architecture of blank and *L. crispatus*-containing scaffolds remain intact after immersion in SVF for 28 d (**Figure 4B**).

In addition, the cumulative and daily release of probiotics from *L. crispatus*-containing scaffolds was evaluated over 4 wk (**Figure 4C and D)**. After 24 hr and 14 d, cumulative probiotic release (and proliferation) from the scaffolds reached 10^8 and $5x10^9$ CFU/mg, while after 28 d, concentrations reached 10^{10} CFU/mg. Daily release showed relatively steady concentrations of approximately 4 $x10^8$ CFU/mg released per day.

Last, the pH-modulation of *L. crispatus*-containing dual- and genipin-only crosslinked scaffolds was assessed by measuring the pH of release eluate after daily media changes (**Figure 4E**). In congruence with release results, a decrease in pH (from 6 to 3.5) was observed from the dual-crosslinked scaffold eluates after ~4 d immersion. Genipin-only scaffolds showed a slightly more gradual decrease in pH, achieving comparable pH levels (3.5) after 5 d. Both scaffolds demonstrated vaginally-relevant pH values after ~4 or 5 d, indicative of probiotic viability and lactic acid production.

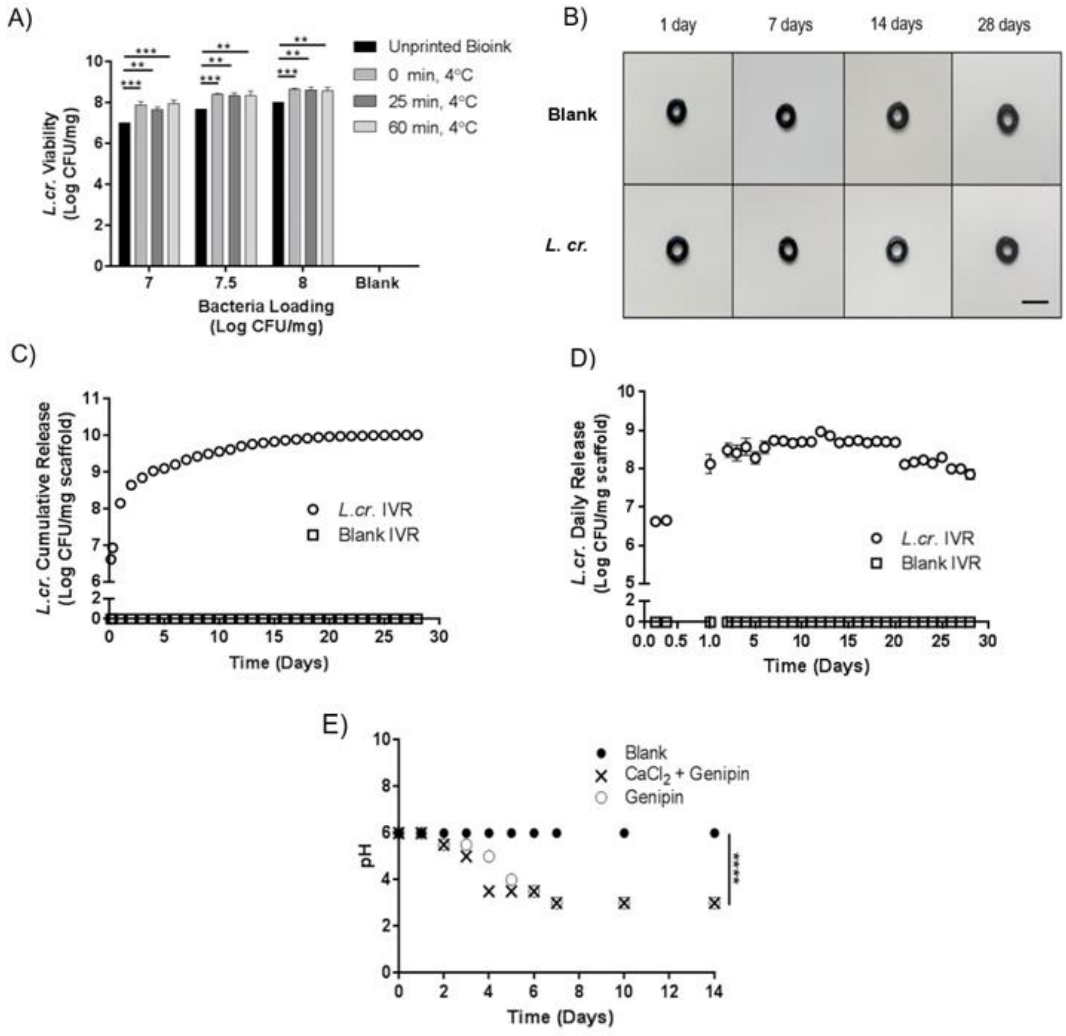

FIGURE 4: SCAFFOLD VIABILITY, STRUCTURAL INTEGRITY, RELEASE, AND MODULATION

Figure 4. Bioprinted scaffolds were assessed for *L. crispatus* viability, structural integrity, cumulative and daily release, and resulting pH modulation. (A) The post-print viability of *L. crispatus*, based on theoretical loadings of $1x10^7$, $5x10^7$, and $1x10^8$ CFU *L. crispatus*/mg scaffold is shown for uncrosslinked scaffolds (relative to unprinted bioinks) that were dissolved in MRS after different durations of crosslinking at 4°C. (B) Representative images of blank or *L. crispatus*-containing (5×10^7 CFU/mg) ring-shaped scaffolds dual-

crosslinked with $CaCl_2$ followed by genipin for 24 hr, and after different immersion durations in SVF (1, 7, 14, 28 d). Scale bar represents 5 mm. (C) The cumulative and (D) daily release and proliferation of *L. crispatus* from crosslinked scaffolds. Values are shown as the mean ± standard deviation from five independent ring-shaped scaffolds. (E) The resulting pH of the release eluate measured and values are shown as the mean ± standard deviation of eluates from three scaffold batches. Error bars are displayed but are smaller than the symbol size. Statistical significance between experimental groups, as calculated by one-way ANOVA, is represented by **$p \leq 0.01$, ***$p \leq 0.001$ and ****$p \leq 0.0001$.

3.5 Stability of *L. crispatus* Release in Scaffolds

The stability of *L. crispatus* was assessed by measuring its release from scaffolds after storage at -20°C, 4°C, and 20°C for 4 wk (**Figure 5**). After storage at -20°C for multiple weeks (**Figure 5A**), scaffolds demonstrated viable probiotic release, similar to freshly made unstored scaffolds. After storage at 4°C, samples stored for 1, 2 and 4 wk showed a slight reduction in viability, relative to fresh scaffolds, but similar viability with respect to each other (**Figure 5B**, $p \leq 0.01$, $p \leq 0.01$, and $p \leq 0.001$, respectively). Lastly, scaffolds stored at room temperature for one week (**Figure 5C**) showed no indication of release and viability, relative to probiotic release from fresh scaffolds, indicating significant decreases in probiotic viability for all storage durations ($p \leq 0.0001$).

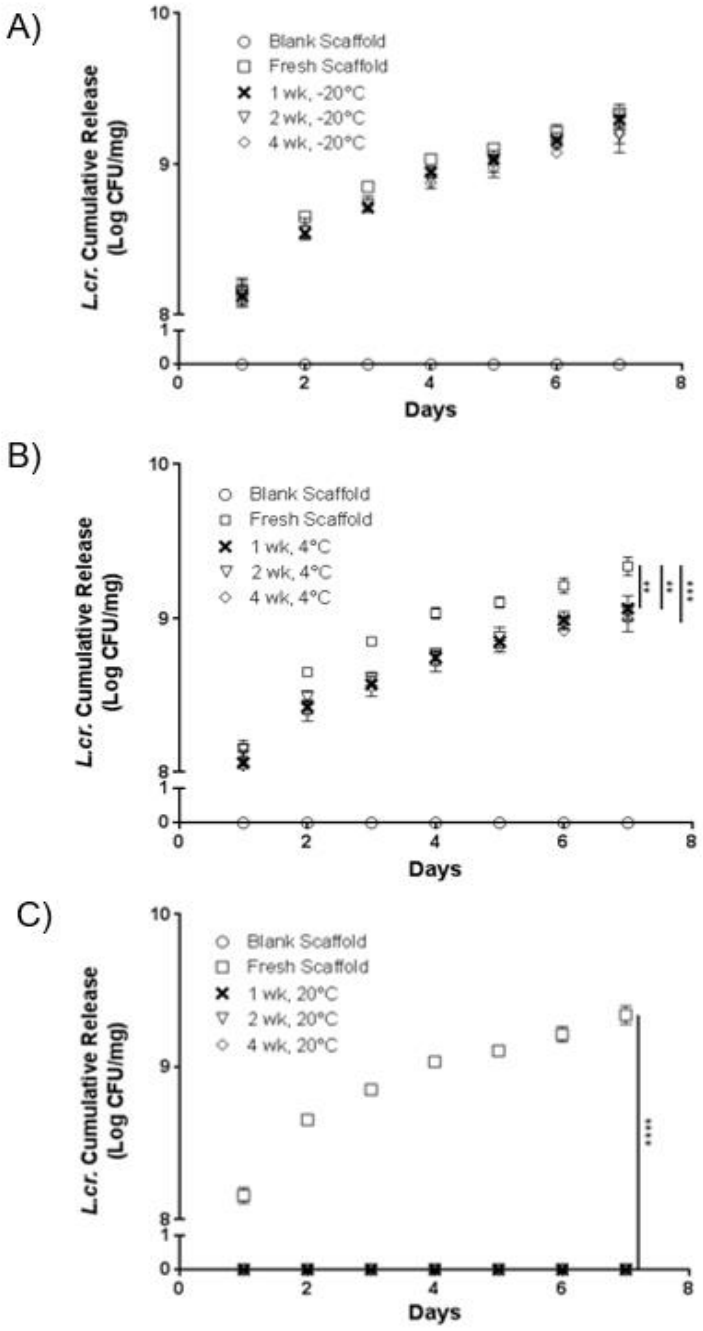

FIGURE 5: SCAFFOLD STABILITY

Figure 5. The stability of dual-crosslinked scaffolds ($CaCl_2$ + genipin, 24 hr) after storage for 1, 2, and 4 wk in (A) freezer (-20 °C), (B) refrigerator (4 °C), and (C) room temperature

(20°C) conditions. Release values are shown as the mean ± standard deviation of *L. crispatus* from the eluates of three independent ring-shaped scaffolds. In some cases, error bars are smaller than the symbol size. Please note overlap in all symbols except for the fresh scaffold in panel C. Statistical significance between experimental groups, as calculated by one-way ANOVA, is represented by **$p \leq 0.01$, ***$p \leq 0.001$, and ****$p \leq 0.0001$.

3.6 Scaffold Characterization

The SEM images of blank and *L. crispatus*-containing scaffolds, dual-crosslinked for 24 hr, are shown in (**Figure 6)**. Proliferation, relative to that in blank scaffolds, was visually evident from cross-sectional images between 1 and 7 d. The presence of *L. crispatus* on the interior cross-section demonstrates the potential of *L. crispatus* to proliferate in the bioprinted scaffolds.

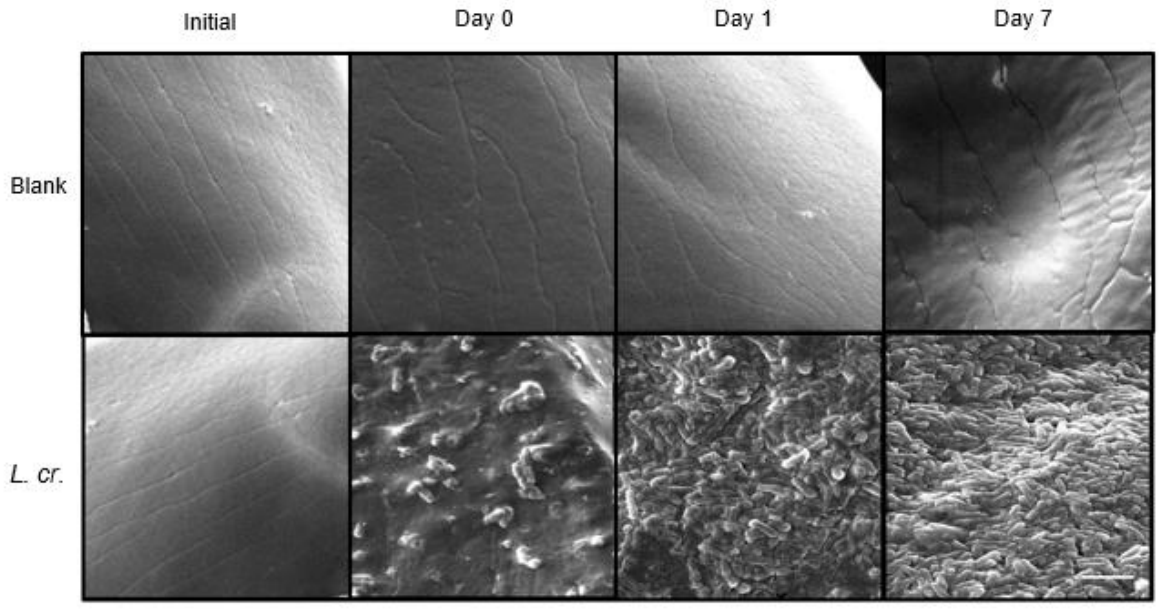

FIGURE 6: SCAFFOLD CROSS SECTION IMAGING

Figure 6. Scanning electron microscopy images of probiotic scaffold loaded with 5×10^7 of *L. crispatus.* Top and bottom images show cross-sections of blank and *L. cr.*-containing scaffolds, respectively. The interior IVR cross-sections are shown after different release time points. Scale bar represents 5 μm.

3.7. VK2/E6E7 Viability

The viability of vaginal keratinocytes (VK2/E6E7) was evaluated after treatment with blank and *L. crispatus*-containing scaffolds, crosslinked with different crosslinkers (**Figure 7**). Vaginal keratinocyte viability was maintained after 24 and 72 hr treatment with all scaffold groups, relative to untreated VK/E6E7 cells. Blank genipin-only and dual-crosslinked *L. crispatus*-containing scaffolds maintained greater than 96% cell viability over 24 and 72 hr treatment conditions. Uncrosslinked and $CaCl_2$-only crosslinked blank scaffolds showed slight increases in viability after 24 and 72 hr, relative to untreated cells ($p \leq 0.01$ (uncrosslinked 24 hr) and $p \leq 0.0001$ (other groups)). In contrast, cell viability for the negative control group, 10% DMSO, had viabilities of 28 and 33% of that observed with untreated cells ($p \leq 0.0001$).

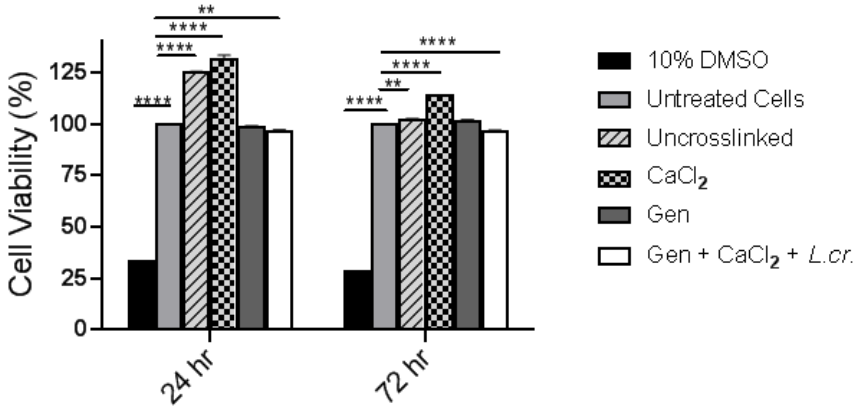

FIGURE 7: CELL VIABILITY

Figure 7. Cell viability of vaginal keratinocytes (VK2/E6E7 cells) that were treated with bioprinted scaffolds for 24 or 72 hr. Negligible cytotoxicity was observed in VK2/E6E7 cells administered IVRs that were processed with different crosslinking conditions. Statistical significance between experimental groups, as calculated by one-way ANOVA, is represented by $^{**}p \leq 0.01$ and $^{****}p \leq 0.0001$.

DISCUSSION

The administration of probiotics has been shown to be a promising new alternative to antibiotics to treat BV[5,32,35,44-46]. Probiotics have been shown to restore and maintain vaginal health by promoting increased immune cell activity, antimicrobial production, reduction of vaginal pH, and competition for nutrients against pathogenic anaerobes in the vaginal microbiome[5,89,90]. Additionally, an increase in cure rate as well as reduction of recurrence has been observed with adjunct probiotic therapy[30,33,47,91,92]. Apart from other probiotic species, *L. crispatus* has seen clinical relevance presumably due to its underlying presence in the healthy vaginal environment. *L. crispatus* has been a prominent probiotic candidate to treat BV and recurrent infections through its ability to produce lactic acid and modulate the acidic pH of the vaginal environment[93,94]. Additionally, *L. crispatus* has been shown to stimulate the release of pro-inflammatory mediators and autophagy in vaginal epithelial cells[95-97].

Although probiotic therapy has shown promise, one of the primary challenges in both oral and intravaginal delivery is in promoting user adherence. In particular, the frequent, once-to-twice daily administration needed for antibiotic and probiotic therapy can result in low user adherence and hence, inadequate treatment outcomes. For this reason, one potential solution is to develop sustained release dosage forms that enable the prolonged delivery of active agents, such as probiotics, over a duration of days to weeks. To date, vaginal tablets, gels/creams, films, capsules, microparticles, intravaginal rings (IVRs), and suppositories have been locally delivered to the female reproductive tract;

however, pod-based IVRs containing lyophilized *L. gasseri*, are the only platform shown to provide sustained probiotic delivery *in vitro*[31,60].

Recently, 3D bioprinting has emerged from additive manufacturing as a new alternative with which to fabricate materials for broad applications including tissue and organ regeneration, biological implants, and drug and biologic delivery[62,67,68,71,72,98,99]. Specifically for the delivery of live cells, bioprinting has shown a highly viable method with which to incorporate and deliver live cells from a variety of materials. In 3D bioprinting, cell-containing bioinks can be extruded at temperatures and pressures that are compatible with physiological conditions, while maintaining cell viability, in an aseptic/sterile environment[100-102]. Due to its success in incorporating both eukaryotic and prokaryotic cells[63-66,69,103,104], we sought to apply bioprinting to develop a novel probiotic-containing scaffold that could prolong probiotic release for durations of days to weeks.

A variety of bioinks have been used for biological printing, some of which include collagen, gelatin, fibronectin, laminin, chitosan, alginate, and silk fibroin[105]. For this initial work, gelatin alginate was selected due to its proven ability in early work to bioprint eukaryotic cells for grafting and regenerative medicine applications[63-66], and more recently to deliver viable and stable prokaryotic cells, while maintaining scaffold integrity[69,103,104]. More broadly, bioprinting has enabled the potential to create precisely designed scaffolds that adopt a streamlined additive manufacturing process, enable the incorporation of biologics, and are relatively inexpensive and rapid to fabricate, relative to custom molding processes[68,69,73]. Furthermore, bioprinting enables the user to customize architectures to

match user preference and to tune release of active agents in personally tailored products. The expansion of bioprinting to female reproductive applications and more specifically infections, may offer a novel and alternative method with which to increase clinical effectiveness, help restore vaginal health, and address recurrent infections in women's health.

In this study, we began by assessing the reproducibility of bioprinting different gelatin alginate formulations with and without the incorporation of probiotics. Bioink homogeneity is an important parameter, first to attain uniform printability and second, to enable nutrient diffusion and hence *L. crispatus* viability in the bioink during and post-printing. First, a variety of gelatin alginate formulations were evaluated to determine the changes in line printing resolution and morphology when *L. crispatus* was incorporated into the bioink[66,76-78]. Of the tested formulations, the 10:2 *L. crispatus*-containing gelatin alginate bioink provided the most accurate line resolution with respect to the specified input line dimensions, with a difference in line width of only 2.5% between the blank and *L. crispatus*-containing 10:2 formulation (**Figure 1B**).

In addition to the fundamentals of maintaining line resolution, bioprinting also relies upon parameters such as infill density, extrusion flow rate and pressure, needle gauge, and layer thickness − which are all contingent on the selected bioink formulation. To investigate the impact of some of these parameters, blank and probiotic-containing lattice structures were bioprinted with a variety of thicknesses and diameters (**Figure 2A-H**). From these lattice structures, the 34G needle printed with the greatest precision, evident

from the achieved infill densities. Overall, it was observed that as the lattice thickness increased, the variation in scaffold thickness from the input value increased (**Figure 2I**), while less variation was seen with changes in the diameter. These results suggest that the weight and viscosity of the bioink may play a more important role in achieving a non-disperse or high-resolution structure. Similarly, as probiotic concentration increased, scaffold thickness increased, while the impact on diameter was only observed with high probiotic loading (blank vs. 10^9, 8 and 15 mm). Overall and as expected, as scaffold thickness increases, more variation in structure may be expected, in particular for more viscous bioinks as seen with *L. crispatus*-containing bioinks. In our hands we found that the 10^7 CFU/mg *L. crispatus*-containing bioink provided prints most closely aligned with the thickness input dimensions. Similar to the findings of other studies, these results indicate that architecture should strive to achieve accurate printing outputs, as prior work has shown that size deviations may induce more rapid release of active agents[59,106] and compromised mechanical integrity.

In parallel with measuring the line resolution of bioprinted lattice structures, bioink viscosity was evaluated to determine the role of the *L. crispatus* inclusion on printing resolution. Similar studies with gelatin alginate have found printability within similar viscosity ranges (~1000 cP) to our 10:2 blank and *L. crispatus*-containing formulations with viscosities of 1171 ± 17 cP and 1616 ± 19 cP at 37°C, respectively[107-109] (**Supplementary Figure 1**). Results from our study are in agreement with rheological studies conducted by other groups that suggest that the viscosity behavior as a function of temperature defines gelatin alginate as a thermosensitive polymer. Its controlled extrusion

through fine needles, while maintaining fidelity in shape, indicates that the bioink act as a non-Newtonian shear thinning fluid[63,87,110-112]. These characteristics contribute to the ability to print fine architectures without compromising cell viability when shear rate changes. Different formulations, including ours and others[78,87,88,113] were shown to have substantial changes in viscosity as function of temperature and concentration, validating the utility of the 10:2 gelatin alginate formulation for bioprinting.

Another component in maintaining scaffold integrity is the impact of the crosslinking agent. With this in mind, bioprinted scaffolds were evaluated using different crosslinkers and crosslinking durations to assess the mechanical integrity of the scaffold over 28 d. Genipin and $CaCl_2$ are known to crosslink gelatin and sodium alginate, respectively [83,85,86,114], however, in our hands, crosslinking with genipin-only resulted in compromised structural integrity by 7 d (**Figure 3A**). Similarly, $CaCl_2$-only scaffolds rapidly degraded within 8 hr. For dual-crosslinked scaffolds, we observed that crosslinking for 24 hr, maintained the highest level of scaffold integrity over 28 d, both visually and with 13% less mass loss than scaffolds crosslinked with genipin-only (**Figure 3B**). These results suggest that dual-crosslinked scaffolds likely require longer crosslinking times to fully harden, and to maintain their shape for longer durations.

In parallel with mass loss studies, the swelling of dual-crosslinked scaffolds was assessed. The dual-crosslinked scaffolds retained more of their initial mass relative to genipin-only crosslinked scaffolds. However, volumetric measurements were difficult to

conduct due to minute changes in scaffold thicknesses and diameters. These data suggest that the scaffold absorbs minimal amounts of surrounding fluid (here, SVF, **Figure 3C**).

From a cellular perspective, cells incorporated via bioprinting are often susceptible to a logarithmic-scale reduction in viability, due to shear stress during the extrusion process[61,110]. Given this, the post-print viability was evaluated to assess the effect of shear stress and temperature, resulting from the extrusion process (**Figure 4A**). Relative to the unprinted bioink, probiotic viability was maintained for all inclusion concentrations and curing durations. Furthermore, a macrostructural evaluation of blank and *L. crispatus*-containing scaffolds showed scaffold integrity after immersion in SVF for 28 d (**Figure 4B**), further emphasizing the formulation selection and ability to bioprint *L. crispatus*-containing scaffolds with similar processing parameters to blank scaffolds. In addition to retaining scaffold integrity over 28 d, sustained *L. crispatus* release was evident through 28 d, culminating in ~5 x 10^9 CFU/mg (**Figure 4C**). Moreover, a daily dose of 1 to 4 x 10^8 CFU/mg was observed through 28 d, demonstrating the potential of the bioprinted scaffolds to release therapeutically relevant probiotic doses, similar to those observed on a daily basis with vaginal tablets and creams/gels. These results indicate that *L. crispatus* remained metabolically active through 28 d and are additionally supported by fiber eluate pH measurements, which showed a decrease to vaginally-relevant levels after three to four days. While lactic acid assays are in the process of being conducted, these pH results indicate the production of lactic acid from the *L. crispatus*[93,94,97]. Hence, the ability to provide sustained release and probiotic proliferation for 28 d, in combination with

corresponding pH modulation, may assist in efforts to restore healthy vaginal conditions and to do so in a way that improves patient adherence.

In addition to assessing probiotic viability and release immediately post-print, the viability and release of probiotics after storage in different conditions was evaluated (**Figure 5**). *L. crispatus* remained viable after 4 wk storage at -20°C, however storage at 4°C resulted in a reduction in release (viability) relative to the fresh scaffold release. In contrast, scaffolds stored at room temperature resulted in non-viable probiotics, indicating that new methods should be considered to improve viability in non-cold chain storage conditions. Improvement in thermostability may be improved by encapsulating probiotic into the core of the scaffold, a method similarly used to fabricate electrospun fibers[115]. The fabrication and distribution of *L. crispatus* into the core of the scaffold is confirmed by cross-sectional SEM images (**Figure 6**) and the presence of *L. crispatus*, seen throughout the scaffold cross-section, provides support for viable proliferation throughout the scaffold, perhaps relating to the consistency observed in daily release. In combination with macrostructural images (**Figures 3 and 4**), dual-crosslinking may help to protect the scaffold from degradation and likely has a role in retaining viability. However, in the future, to help increase probiotic viability in more challenging, metabolically-active (room temperature) storage conditions, additives, such as, xylitol, whey protein, sucrose fatty acid esters, and primarily, magnesium stearate, may be used to maintain or increase viability, as shown in previous thermostability studies[116,117].

Additionally, while crosslinking is necessary to maintain the mechanical integrity of gelatin alginate scaffolds, it can be challenging to find crosslinkers that exert minimal toxicity on prokaryotic and eukaryotic cells, in particular when cells are printed within the scaffolds. Moreover finding the ideal combination of bioink and crosslinker can be challenging and may compromise safety and mechanical integrity. While $CaCl_2$ has been found to be a cytocompatible crosslinker for alginate[83,118], most current methods of gelatin crosslinking are cytotoxic. Notably, the most popular gelatin crosslinking reagent, glutaraldehyde, can be toxic if it is biodegraded and released in the body[119]. In comparison, genipin has been shown to be a safer alternative to improve the mechanical and thermal properties of gelatin, as well as prolong its degradation time[81]. Despite the concurred safety of genipin, there have been some concerns regarding acute and dose-dependent toxicity[120]. For this reason, scaffolds crosslinked with a variety of crosslinking reagents were tested for cytotoxicity after administration to vaginal epithelial cells (**Figure 7**). Negligible toxicity was observed after treatment with genipin-crosslinked and all groups, indicating preliminary promise *in vitro* with the concentrations tested. In future studies, it will be important to evaluate the biocompatibility of bioprinted scaffolds in *ex vivo* and *in vivo* systems. To improve crosslinking formulation, a lower genipin concentrations may be evaluated to provide an even safer application.

The goals of this study were to develop and characterize a 3D-bioprinted probiotic-containing sustained release intravaginal dosage form. The 10:2 gelatin alginate formulation, demonstrated fine printing resolution, in addition to mechanical integrity over 28 d. Additionally, bioprinted scaffolds demonstrated high *L. crispatus* loading, maintained

viability over different curing and storage conditions, and demonstrated cumulative and daily release values that are within the range of required dosing for intravaginal applications. Furthermore, from the preliminary *in vitro* studies conducted here, vaginal cell viability was maintained, indicating the potential for 3D-bioprinted scaffolds to advance to *in vitro*, *ex vivo*, and *in vivo* studies. This study highlights the potential of 3D-bioprinted scaffolds for future female reproductive infections and health applications, showing promise in providing a new alternative for sustained probiotic delivery.

REFERENCES

1. Haahr, T. *et al.* Abnormal vaginal microbiota may be associated with poor reproductive outcomes: a prospective study in IVF patients. *Hum Reprod* **31**, 795-803, doi:10.1093/humrep/dew026 (2016).
2. Nasioudis, D., Linhares, I. M., Ledger, W. J. & Witkin, S. S. Bacterial vaginosis: a critical analysis of current knowledge. *Bjog* **124**, 61-69, doi:10.1111/1471-0528.14209 (2017).
3. Peebles, K., Velloza, J., Balkus, J. E., McClelland, R. S. & Barnabas, R. V. High Global Burden and Costs of Bacterial Vaginosis: A Systematic Review and Meta-Analysis. *Sex Transm Dis* **46**, 304-311, doi:10.1097/olq.0000000000000972 (2019).
4. Machado, D., Castro, J., Palmeira-de-Oliveira, A., Martinez-de-Oliveira, J. & Cerca, N. Bacterial Vaginosis Biofilms: Challenges to Current Therapies and Emerging Solutions. *Frontiers in microbiology* **6**, 1528, doi:10.3389/fmicb.2015.01528 (2015).
5. Mastromarino, P., Vitali, B. & Mosca, L. Bacterial vaginosis: a review on clinical trials with probiotics. *The new microbiologica* **36**, 229-238 (2013).
6. Menard, J. P. Antibacterial treatment of bacterial vaginosis: current and emerging therapies. *International journal of women's health* **3**, 295-305, doi:10.2147/IJWH.S23814 (2011).
7. Verstraelen, H., Vervaet, C. & Remon, J. P. Rationale and Safety Assessment of a Novel Intravaginal Drug-Delivery System with Sustained DL-Lactic Acid Release, Intended for Long-Term Protection of the Vaginal Microbiome. *PloS one* **11**, e0153441, doi:10.1371/journal.pone.0153441 (2016).
8. Brotman, R. M. *et al.* Bacterial vaginosis assessed by gram stain and diminished colonization resistance to incident gonococcal, chlamydial, and trichomonal genital infection. *The Journal of infectious diseases* **202**, 1907-1915, doi:10.1086/657320 (2010).
9. Wiesenfeld, H. C., Hillier, S. L., Krohn, M. A., Landers, D. V. & Sweet, R. L. Bacterial vaginosis is a strong predictor of Neisseria gonorrhoeae and Chlamydia trachomatis infection. *Clin Infect Dis* **36**, 663-668 (2003).
10. Wiesenfeld, H. C. *et al.* Lower genital tract infection and endometritis: insight into subclinical pelvic inflammatory disease. *Obstetrics and gynecology* **100**, 456-463 (2002).
11. Watts, D. H., Krohn, M. A., Hillier, S. L. & Eschenbach, D. A. Bacterial vaginosis as a risk factor for post-cesarean endometritis. *Obstetrics and gynecology* **75**, 52-58 (1990).
12. Leitich, H. & Kiss, H. Asymptomatic bacterial vaginosis and intermediate flora as risk factors for adverse pregnancy outcome. *Best Pract Res Clin Obstet Gynaecol* **21**, 375-390, doi:10.1016/j.bpobgyn.2006.12.005 (2007).
13. Leitich, H. *et al.* Bacterial vaginosis as a risk factor for preterm delivery: a meta-analysis. *Am J Obstet Gynecol* **189**, 139-147 (2003).
14. Silver, H. M., Sperling, R. S., St Clair, P. J. & Gibbs, R. S. Evidence relating bacterial vaginosis to intraamniotic infection. *Am J Obstet Gynecol* **161**, 808-812 (1989).
15. DiGiulio, D. B. Diversity of microbes in amniotic fluid. *Seminars in fetal & neonatal medicine* **17**, 2-11, doi:10.1016/j.siny.2011.10.001 (2012).
16. DiGiulio, D. B. *et al.* Prevalence and diversity of microbes in the amniotic fluid, the fetal inflammatory response, and pregnancy outcome in women with preterm pre-labor rupture of membranes. *Am J Reprod Immunol* **64**, 38-57, doi:10.1111/j.1600-0897.2010.00830.x (2010).

17. Berardi-Grassias, L., Roy, O., Berardi, J. C. & Furioli, J. Neonatal meningitis due to Gardnerella vaginalis. *European journal of clinical microbiology & infectious diseases : official publication of the European Society of Clinical Microbiology* **7**, 406-407 (1988).
18. Hillier, S. L. *et al.* A case-control study of chorioamnionic infection and histologic chorioamnionitis in prematurity. *The New England journal of medicine* **319**, 972-978, doi:10.1056/NEJM198810133191503 (1988).
19. Holst, E., Goffeng, A. R. & Andersch, B. Bacterial vaginosis and vaginal microorganisms in idiopathic premature labor and association with pregnancy outcome. *Journal of clinical microbiology* **32**, 176-186 (1994).
20. Goldenberg, R. L. *et al.* Bacterial colonization of the vagina during pregnancy in four ethnic groups. Vaginal Infections and Prematurity Study Group. *Am J Obstet Gynecol* **174**, 1618-1621, doi:S0002937896002451 [pii] (1996).
21. Rezeberga, D., Lazdane, G., Kroica, J., Sokolova, L. & Donders, G. G. Placental histological inflammation and reproductive tract infections in a low risk pregnant population in Latvia. *Acta Obstet Gynecol Scand* **87**, 360-365, doi:791034371 [pii] 10.1080/00016340801936487 (2008).
22. Svare, J. A., Schmidt, H., Hansen, B. B. & Lose, G. Bacterial vaginosis in a cohort of Danish pregnant women: prevalence and relationship with preterm delivery, low birthweight and perinatal infections. *Bjog* **113**, 1419-1425, doi:BJO1087 [pii] 10.1111/j.1471-0528.2006.01087.x (2006).
23. Zhang, X. *et al.* [Relationship between vaginal sialidase bacteria vaginosis and chorioammionitis]. *Zhonghua fu chan ke za zhi* **37**, 588-590 (2002).
24. Hitti, J. *et al.* Vaginal indicators of amniotic fluid infection in preterm labor. *Obstetrics and gynecology* **97**, 211-219 (2001).
25. MacPhee, R. A., Hummelen, R., Bisanz, J. E., Miller, W. L. & Reid, G. Probiotic strategies for the treatment and prevention of bacterial vaginosis. *Expert Opin Pharmacother* **11**, 2985-2995, doi:10.1517/14656566.2010.512004 (2010).
26. Machado, D., Castro, J., Palmeira-de-Oliveira, A., Martinez-de-Oliveira, J. & Cerca, N. Bacterial Vaginosis Biofilms: Challenges to Current Therapies and Emerging Solutions. *Front Microbiol* **6**, 1528, doi:10.3389/fmicb.2015.01528 (2015).
27. Bradshaw, C. S. *et al.* High recurrence rates of bacterial vaginosis over the course of 12 months after oral metronidazole therapy and factors associated with recurrence. *The Journal of infectious diseases* **193**, 1478-1486, doi:10.1086/503780 (2006).
28. Palmeira-de-Oliveira, R., Palmeira-de-Oliveira, A. & Martinez-de-Oliveira, J. New strategies for local treatment of vaginal infections. *Adv Drug Deliv Rev* **92**, 105-122, doi:10.1016/j.addr.2015.06.008 (2015).
29. Borges, S., Silva, J. & Teixeira, P. The role of lactobacilli and probiotics in maintaining vaginal health. *Archives of Gynecology and Obstetrics* **289**, 479-489, doi:10.1007/s00404-013-3064-9 (2014).
30. Recine, N. *et al.* Restoring vaginal microbiota: biological control of bacterial vaginosis. A prospective case–control study using Lactobacillus rhamnosus BMX 54 as adjuvant treatment against bacterial vaginosis. *Archives of Gynecology and Obstetrics* **293**, 101-107, doi:10.1007/s00404-015-3810-2 (2016).
31. Chandrashekhar, P., Minooei, F., Arreguin, W., Masigol, M. & Steinbach-Rankins, J. M. Perspectives on Existing and Novel Alternative Intravaginal Probiotic Delivery Methods

in the Context of Bacterial Vaginosis Infection. *The AAPS Journal* **23**, doi:10.1208/s12248-021-00602-z (2021).
32. Wang, Z., He, Y. & Zheng, Y. Probiotics for the Treatment of Bacterial Vaginosis: A Meta-Analysis. *International Journal of Environmental Research and Public Health* **16**, 3859, doi:10.3390/ijerph16203859 (2019).
33. Wijgert, J. & Verwijs, M. Lactobacilli-containing vaginal probiotics to cure or prevent bacterial or fungal vaginal dysbiosis: a systematic review and recommendations for future trial designs. *BJOG: An International Journal of Obstetrics & Gynaecology* **127**, 287-299, doi:10.1111/1471-0528.15870 (2020).
34. Muzny, C. A. & Kardas, P. A Narrative Review of Current Challenges in the Diagnosis and Management of Bacterial Vaginosis. *Sex Transm Dis* **47**, 441-446, doi:10.1097/olq.0000000000001178 (2020).
35. Faught, B. M. & Reyes, S. Characterization and Treatment of Recurrent Bacterial Vaginosis. *J Womens Health (Larchmt)* **28**, 1218-1226, doi:10.1089/jwh.2018.7383 (2019).
36. Coudray, M. S. & Madhivanan, P. Bacterial vaginosis-A brief synopsis of the literature. *Eur J Obstet Gynecol Reprod Biol* **245**, 143-148, doi:10.1016/j.ejogrb.2019.12.035 (2020).
37. Vodstrcil, L. A., Muzny, C. A., Plummer, E. L., Sobel, J. D. & Bradshaw, C. S. Bacterial vaginosis: drivers of recurrence and challenges and opportunities in partner treatment. *BMC Medicine* **19**, doi:10.1186/s12916-021-02077-3 (2021).
38. Bohbot, J. M. *et al.* Efficacy and safety of vaginally administered lyophilized Lactobacillus crispatus IP 174178 in the prevention of bacterial vaginosis recurrence. *J Gynecol Obstet Hum Reprod* **47**, 81-86, doi:10.1016/j.jogoh.2017.11.005 (2018).
39. Cianci, A. *et al.* Observational prospective study on Lactobacillus plantarum P 17630 in the prevention of vaginal infections, during and after systemic antibiotic therapy or in women with recurrent vaginal or genitourinary infections. *J Obstet Gynaecol* **38**, 693-696, doi:10.1080/01443615.2017.1399992 (2018).
40. Ngugi, B. M. *et al.* Effects of bacterial vaginosis-associated bacteria and sexual intercourse on vaginal colonization with the probiotic Lactobacillus crispatus CTV-05. *Sex Transm Dis* **38**, 1020-1027, doi:10.1097/OLQ.0b013e3182267ac4 (2011).
41. Tomás, M., Palmeira-de-Oliveira, A., Simões, S., Martinez-de-Oliveira, J. & Palmeira-de-Oliveira, R. Bacterial vaginosis: Standard treatments and alternative strategies. *Int J Pharm* **587**, 119659, doi:10.1016/j.ijpharm.2020.119659 (2020).
42. Homayouni, A. *et al.* Effects of probiotics on the recurrence of bacterial vaginosis: a review. *Journal of lower genital tract disease* **18**, 79-86, doi:10.1097/LGT.0b013e31829156ec (2014).
43. Mastromarino, P. *et al.* Effectiveness of Lactobacillus-containing vaginal tablets in the treatment of symptomatic bacterial vaginosis. *Clin Microbiol Infect* **15**, 67-74, doi:10.1111/j.1469-0691.2008.02112.x (2009).
44. Mohammed, L. *et al.* Live Bacteria Supplementation as Probiotic for Managing Fishy, Odorous Vaginal Discharge Disease of Bacterial Vaginosis: An Alternative Treatment Option? *Cureus* **12**, e12362, doi:10.7759/cureus.12362 (2020).
45. Tidbury, F. D., Langhart, A., Weidlinger, S. & Stute, P. Non-antibiotic treatment of bacterial vaginosis—a systematic review. *Archives of Gynecology and Obstetrics* **303**, 37-45, doi:10.1007/s00404-020-05821-x (2021).
46. Mizgier, M., Jarzabek-Bielecka, G., Mruczyk, K. & Kedzia, W. The role of diet and probiotics in prevention and treatment of bacterial vaginosis and vulvovaginal candidiasis in

adolescent girls and non-pregnant women. *Ginekologia Polska* **91**, 412-416, doi:10.5603/gp.2020.0070 (2020).
47. Larsson, P. G., Stray-Pedersen, B., Ryttig, K. R. & Larsen, S. Human lactobacilli as supplementation of clindamycin to patients with bacterial vaginosis reduce the recurrence rate; a 6-month, double-blind, randomized, placebo-controlled study. *BMC Womens Health* **8**, 3, doi:10.1186/1472-6874-8-3 (2008).
48. Cohen, C. R. *et al.* Randomized Trial of Lactin-V to Prevent Recurrence of Bacterial Vaginosis. *The New England journal of medicine* **382**, 1906-1915, doi:10.1056/NEJMoa1915254 (2020).
49. Lai, S. K., Wang, Y. Y., Hida, K., Cone, R. & Hanes, J. Nanoparticles reveal that human cervicovaginal mucus is riddled with pores larger than viruses. *Proceedings of the National Academy of Sciences of the United States of America* **107**, 598-603, doi:10.1073/pnas.0911748107 (2010).
50. Ensign, L. M., Cone, R. & Hanes, J. Nanoparticle-based drug delivery to the vagina: a review. *Journal of controlled release : official journal of the Controlled Release Society* **190**, 500-514, doi:10.1016/j.jconrel.2014.04.033 (2014).
51. Baelo, A. *et al.* Disassembling bacterial extracellular matrix with DNase-coated nanoparticles to enhance antibiotic delivery in biofilm infections. *Journal of controlled release : official journal of the Controlled Release Society* **209**, 150-158, doi:10.1016/j.jconrel.2015.04.028 (2015).
52. Bartley, J. B. *et al.* Personal digital assistants used to document compliance of bacterial vaginosis treatment. *Sex Transm Dis* **31**, 488-491, doi:10.1097/01.olq.0000135990.21755.51 (2004).
53. Chee, W. J. Y., Chew, S. Y. & Than, L. T. L. Vaginal microbiota and the potential of Lactobacillus derivatives in maintaining vaginal health. *Microbial Cell Factories* **19**, doi:10.1186/s12934-020-01464-4 (2020).
54. Gunawardana, M. *et al.* Sustained delivery of commensal bacteria from pod-intravaginal rings. *Antimicrob Agents Chemother* **58**, 2262-2267, doi:10.1128/aac.02542-13 (2014).
55. Vuotto, C., Longo, F. & Donelli, G. Probiotics to counteract biofilm-associated infections: promising and conflicting data. *International Journal of Oral Science* **6**, 189-194, doi:10.1038/ijos.2014.52 (2014).
56. Cheow, W. S. & Hadinoto, K. Biofilm-like Lactobacillus rhamnosus probiotics encapsulated in alginate and carrageenan microcapsules exhibiting enhanced thermotolerance and freeze-drying resistance. *Biomacromolecules* **14**, 3214-3222, doi:10.1021/bm400853d (2013).
57. Jones, S. E. & Versalovic, J. Probiotic Lactobacillus reuteri biofilms produce antimicrobial and anti-inflammatory factors. *BMC Microbiology* **9**, 35, doi:10.1186/1471-2180-9-35 (2009).
58. Asvadi, N. H., Dang, N. T., Davis-Poynter, N. & Coombes, A. G. Evaluation of microporous polycaprolactone matrices for controlled delivery of antiviral microbicides to the female genital tract. *J Mater Sci Mater Med* **24**, 2719-2727, doi:10.1007/s10856-013-5010-6 (2013).
59. Baum, M. M. *et al.* An intravaginal ring for the simultaneous delivery of multiple drugs. *J Pharm Sci* **101**, 2833-2843, doi:10.1002/jps.23208 (2012).

60. Gunawardana, M., Baum, M. M., Smith, T. J. & Moss, J. A. An intravaginal ring for the sustained delivery of antibodies. *J Pharm Sci* **103**, 3611-3620, doi:10.1002/jps.24154 (2014).
61. Emmermacher, J. *et al.* Engineering considerations on extrusion-based bioprinting: interactions of material behavior, mechanical forces and cells in the printing needle. *Biofabrication* **12**, 025022, doi:10.1088/1758-5090/ab7553 (2020).
62. Matai, I., Kaur, G., Seyedsalehi, A., McClinton, A. & Laurencin, C. T. Progress in 3D bioprinting technology for tissue/organ regenerative engineering. *Biomaterials* **226**, 119536, doi:10.1016/j.biomaterials.2019.119536 (2020).
63. Rastogi, P. & Kandasubramanian, B. Review of alginate-based hydrogel bioprinting for application in tissue engineering. *Biofabrication* **11**, 042001, doi:10.1088/1758-5090/ab331e (2019).
64. Liu, P. *et al.* 3D bioprinting and in vitro study of bilayered membranous construct with human cells-laden alginate/gelatin composite hydrogels. *Colloids Surf B Biointerfaces* **181**, 1026-1034, doi:10.1016/j.colsurfb.2019.06.069 (2019).
65. Chen, Q. *et al.* An Interpenetrating Alginate/Gelatin Network for Three-Dimensional (3D) Cell Cultures and Organ Bioprinting. *Molecules* **25**, 756, doi:10.3390/molecules25030756 (2020).
66. Shi, L. *et al.* Three-dimensional printing alginate/gelatin scaffolds as dermal substitutes for skin tissue engineering. *Polymer Engineering & Science* **58**, 1782-1790, doi:10.1002/pen.24779 (2018).
67. Mohammadi, Z. & Rabbani, M. Bacterial Bioprinting on a Flexible Substrate for Fabrication of a Colorimetric Temperature Indicator by Using a Commercial Inkjet Printer. *J Med Signals Sens* **8**, 170-174, doi:10.4103/jmss.JMSS_41_17 (2018).
68. Dubbin, K. *et al.* Projection Microstereolithographic Microbial Bioprinting for Engineered Biofilms. *Nano Letters* **21**, 1352-1359, doi:10.1021/acs.nanolett.0c04100 (2021).
69. Lehner, B. A. E., Schmieden, D. T. & Meyer, A. S. A Straightforward Approach for 3D Bacterial Printing. *ACS Synth Biol* **6**, 1124-1130, doi:10.1021/acssynbio.6b00395 (2017).
70. Rodríguez-Dévora, J. I., Zhang, B., Reyna, D., Shi, Z.-D. & Xu, T. High throughput miniature drug-screening platform using bioprinting technology. *Biofabrication* **4**, 035001, doi:10.1088/1758-5082/4/3/035001 (2012).
71. Ning, E. *et al.* 3D bioprinting of mature bacterial biofilms for antimicrobial resistance drug testing. *Biofabrication* **11**, 045018, doi:10.1088/1758-5090/ab37a0 (2019).
72. Schmieden, D. T. *et al.* Printing of Patterned, Engineered E. coli Biofilms with a Low-Cost 3D Printer. *ACS Synth Biol* **7**, 1328-1337, doi:10.1021/acssynbio.7b00424 (2018).
73. Balasubramanian, S., Aubin-Tam, M. E. & Meyer, A. S. 3D Printing for the Fabrication of Biofilm-Based Functional Living Materials. *ACS Synth Biol* **8**, 1564-1567, doi:10.1021/acssynbio.9b00192 (2019).
74. Zhang, L., Lou, Y. & Schutyser, M. 3D printing of cereal-based food structures containing probiotics. *Food Structure* **18**, 14-22 (2018).
75. Owen, D. H. & Katz, D. F. A vaginal fluid simulant. *Contraception* **59**, 91-95, doi:10.1016/s0010-7824(99)00010-4 (1999).
76. Wu, Z. *et al.* Bioprinting three-dimensional cell-laden tissue constructs with controllable degradation. *Sci Rep* **6**, 24474, doi:10.1038/srep24474 (2016).

77. Huang, S., Yao, B., Xie, J. & Fu, X. 3D bioprinted extracellular matrix mimics facilitate directed differentiation of epithelial progenitors for sweat gland regeneration. *Acta Biomater* **32**, 170-177, doi:10.1016/j.actbio.2015.12.039 (2016).
78. Duan, B., Hockaday, L. A., Kang, K. H. & Butcher, J. T. 3D bioprinting of heterogeneous aortic valve conduits with alginate/gelatin hydrogels. *J Biomed Mater Res A* **101**, 1255-1264, doi:10.1002/jbm.a.34420 (2013).
79. Li, Z. *et al.* Tuning Alginate-Gelatin Bioink Properties by Varying Solvent and Their Impact on Stem Cell Behavior. *Scientific Reports* **8**, doi:10.1038/s41598-018-26407-3 (2018).
80. Muzzarelli, R. A., El Mehtedi, M., Bottegoni, C., Aquili, A. & Gigante, A. Genipin-Crosslinked Chitosan Gels and Scaffolds for Tissue Engineering and Regeneration of Cartilage and Bone. *Mar Drugs* **13**, 7314-7338, doi:10.3390/md13127068 (2015).
81. Bigi, A., Cojazzi, G., Panzavolta, S., Roveri, N. & Rubini, K. Stabilization of gelatin films by crosslinking with genipin. *Biomaterials* **23**, 4827-4832, doi:10.1016/s0142-9612(02)00235-1 (2002).
82. Hariyadi, D., Hendradi, E., Purwanti, T., Fadil, F. D. G. P. & Ramadani, C. N. Effect of cross linking agent and polymer on the characteristics of ovalbumin loaded alginate microspheres. *International Journal of Pharmacy and Pharmaceutical Sciences* **6**, 469-474 (2014).
83. Saarai, A., Kbapárková, V., Sedlacek, T. & Sáha, P. A comparative study of crosslinked sodium alginate/gelatin hydrogels for wound dressing. (2011)
84. Seixas, F. L., Turbiani, F., Salomao, P. G., Souza, R. P. & Gimenes, M. L. Biofilms Composed of Alginate and Pectin: Effect of Concentration of Crosslinker and Plasticizer Agents. *Chemical engineering transactions* **32**, 1693-1698 (2013).
85. Ma, W., Yin, S.-W., Yang, X.-Q. & Qi, J.-R. Genipin-crosslinked gelatin films as controlled releasing carriers of lysozyme. *Food Research International* **51**, 321–324, doi:10.1016/j.foodres.2012.12.039 (2013).
86. Gorczyca, G. *et al.* Preparation and characterization of genipin cross-linked porous chitosan-collagen-gelatin scaffolds using chitosan-CO2 solution. *Carbohydr Polym* **102**, 901-911, doi:10.1016/j.carbpol.2013.10.060 (2014).
87. Ouyang, L., Yao, R., Zhao, Y. & Sun, W. Effect of bioink properties on printability and cell viability for 3D bioplotting of embryonic stem cells. *Biofabrication* **8**, 035020, doi:10.1088/1758-5090/8/3/035020 (2016).
88. Giuseppe, M. D. *et al.* Mechanical behaviour of alginate-gelatin hydrogels for 3D bioprinting. *J Mech Behav Biomed Mater* **79**, 150-157, doi:10.1016/j.jmbbm.2017.12.018 (2018).
89. Aroutcheva, A. & et al. Defense factors of vaginal lactobacilli. *American Journal of Obstetrics and Gynecology* **185**, 375 (2001).
90. Borchers, A. T. & et al. Probiotics and immunity. *Journal of Gastroenterology* **44**, 26 (2009).
91. Anukam, K. *et al.* Augmentation of antimicrobial metronidazole therapy of bacterial vaginosis with oral probiotic Lactobacillus rhamnosus GR-1 and Lactobacillus reuteri RC-14: randomized, double-blind, placebo controlled trial. *Microbes Infect* **8**, 1450-1454, doi:10.1016/j.micinf.2006.01.003 (2006).
92. Bodean, O., Munteanu, O., Cirstoiu, C., Secara, D. & Cirstoiu, M. Probiotics--a helpful additional therapy for bacterial vaginosis. *J Med Life* **6**, 434-436 (2013).
93. Witkin, S. S. *et al.* Influence of vaginal bacteria and D- and L-lactic acid isomers on vaginal extracellular matrix metalloproteinase inducer: implications for protection against upper genital tract infections. *mBio* **4**, doi:10.1128/mBio.00460-13 (2013).

94. Borgogna, J.-L. C. *et al.* Biogenic Amines Increase the Odds of Bacterial Vaginosis and Affect the Growth of and Lactic Acid Production by Vaginal Lactobacillus spp. *Applied and Environmental Microbiology* **87**, doi:10.1128/aem.03068-20 (2021).
95. Witkin, S. S. & Linhares, I. M. Why do lactobacilli dominate the human vaginal microbiota? *Bjog* **124**, 606-611, doi:10.1111/1471-0528.14390 (2017).
96. Aldunate, M. & et al. Antimicrobial and immune modulatory effects of lactic acid and short chain fatty acids produced by vaginal microbiota associated with eubiosis and bacterial vaginosis. *Frontiers in Physiology* **6** (2015).
97. Abdelmaksoud, A. A. *et al.* Comparison of Lactobacillus crispatus isolates from Lactobacillus-dominated vaginal microbiomes with isolates from microbiomes containing bacterial vaginosis-associated bacteria. *Microbiology* **162**, 466-475, doi:10.1099/mic.0.000238 (2016).
98. Yan, W. C. *et al.* 3D bioprinting of skin tissue: From pre-processing to final product evaluation. *Adv Drug Deliv Rev* **132**, 270-295, doi:10.1016/j.addr.2018.07.016 (2018).
99. Luis, E. *et al.* 3D Direct Printing of Silicone Meniscus Implant Using a Novel Heat-Cured Extrusion-Based Printer. *Polymers (Basel)* **12**, doi:10.3390/polym12051031 (2020).
100. Shapira, A. & Dvir, T. 3D Tissue and Organ Printing—Hope and Reality. *Advanced Science* **8**, 2003751, doi:10.1002/advs.202003751 (2021).
101. Gu, Z. & et al. Development of 3D bioprinting: From printing methods to biomedical applications. *Asian Journal of Pharmaceutical Sciences* **15**, 529 (2020).
102. Gungor-Ozkerim, P. S., Inci, I., Zhang, Y. S., Khademhosseini, A. & Dokmeci, M. R. Bioinks for 3D bioprinting: an overview. *Biomaterials Science* **6**, 915-946, doi:10.1039/c7bm00765e (2018).
103. Connell, J. L. & et al. 3D printing of microscopic bacterial communities. *Proceedings of the National Academy of Sciences of the United States of America* **110**, 18380 (2013).
104. Joshi, S., Cook, E. & Mannoor, M. S. Bacterial Nanobionics via 3D Printing. *Nano Lett* **18**, 7448-7456, doi:10.1021/acs.nanolett.8b02642 (2018).
105. Mandrycky, C., Wang, Z., Kim, K. & Kim, D. H. 3D bioprinting for engineering complex tissues. *Biotechnol Adv* **34**, 422-434, doi:10.1016/j.biotechadv.2015.12.011 (2016).
106. Malcolm, R. K. & et al. Advances in microbicide vaginal rings. *Antiviral Research* **88**, 30 (2010).
107. Paxton, N. *et al.* Proposal to assess printability of bioinks for extrusion-based bioprinting and evaluation of rheological properties governing bioprintability. *Biofabrication* **9**, 044107, doi:10.1088/1758-5090/aa8dd8 (2017).
108. Wüst, S., Godla, M. E., Müller, R. & Hofmann, S. Tunable hydrogel composite with two-step processing in combination with innovative hardware upgrade for cell-based three-dimensional bioprinting. *Acta Biomaterialia* **10**, 630-640, doi:10.1016/j.actbio.2013.10.016 (2014).
109. Augst, A. D., Kong, H. J. & Mooney, D. J. Alginate Hydrogels as Biomaterials. *Macromolecular Bioscience* **6**, 623 (2006).
110. Gómez-Blanco, J. C. *et al.* Bioink Temperature Influence on Shear Stress, Pressure and Velocity Using Computational Simulation. *Processes* **8**, 865, doi:10.3390/pr8070865 (2020).
111. Gao, T. *et al.* Optimization of gelatin–alginate composite bioink printability using rheological parameters: a systematic approach. *Biofabrication* **10**, 034106, doi:10.1088/1758-5090/aacdc7 (2018).

112. Cooke, M. E. & Rosenzweig, D. H. The rheology of direct and suspended extrusion bioprinting. *APL Bioengineering* **5**, 011502, doi:10.1063/5.0031475 (2021).
113. Bociaga, D., Bartniak, M., Grabarczyk, J. & Przybyszewska, K. Sodium Alginate/Gelatine Hydrogels for Direct Bioprinting—The Effect of Composition Selection and Applied Solvents on the Bioink Properties. *Materials* **12**, 2669, doi:10.3390/ma12172669 (2019).
114. Erdagi, S. I., Ngwabebhoh, F. A. & Yildiz, U. Genipin crosslinked gelatin-diosgenin-nanocellulose hydrogels for potential wound dressing and healing applications. *International Journal of Biological Macromolecules* **149**, 651 (2020).
115. Feng, K. & et al. Improved Viability and Thermal Stability of the Probiotics Encapsulated in a Novel Electrospun Fiber Mat. *Journal of Agricultural and Food Chemistry* **66**, 10890 (2018).
116. Kang, M.-S., Kim, Y.-S., Lee, H.-C., Lim, H.-S. & Oh, J.-S. Comparison of Temperature and Additives Affecting the Stability of the ProbioticWeissella cibaria. *Chonnam Medical Journal* **48**, 159, doi:10.4068/cmj.2012.48.3.159 (2012).
117. Çaglar, E. & et al. Effect of chewing gums containing xylitol or probiotic bacteria on salivary mutans streptococci and lactobacilli. *Clinical Oral Investigations* **11**, 425 (2007).
118. Kuo, C. K. & Ma, P. X. Maintaining dimensions and mechanical properties of ionically crosslinked alginate hydrogel scaffolds in vitro. *J Biomed Mater Res A* **84**, 899-907, doi:10.1002/jbm.a.31375 (2008).
119. Reddy, N., Reddy, R. & Jiang, Q. Crosslinking biopolymers for biomedical applications. *Trends Biotechnol* **33**, 362-369, doi:10.1016/j.tibtech.2015.03.008 (2015).
120. Wang, C., Lau, T. T., Loh, W. L., Su, K. & Wang, D. A. Cytocompatibility study of a natural biomaterial crosslinker--Genipin with therapeutic model cells. *J Biomed Mater Res B Appl Biomater* **97**, 58-65, doi:10.1002/jbm.b.31786 (2011).

VITA

Anthony Kyser was born on June 27th, 1997 in Bakersfield, California. He has lived in Louisville, Kentucky for 15 years. During his undergraduate, he worked for Leica Biosystems, Norton Healthcare, and Eccrine Systems. Anthony graduated with his Bachelors of Science degree in Bioengineering at the University of Louisville in 2020. He enjoys running and spending time with friends and family.